BYG·DTU

DANMARKS
TEKNISKE
UNIVERSITET

DTU

Center for ARKTISK TEKNOLOGI

Bæredygtigt arktisk byggeri i det 21. århundrede

Vakuumrørsolfangere – Statusrapport 2 til
VILLUM KANN RASMUSSEN FONDEN

Sagsrapport
BYG·DTU SR-05-05
2005
ISSN 1601 - 8605

Bæredygtigt arktisk byggeri i det 21. århundrede

Vakuumrørsolfangere – Statusrapport 2 til
VILLUM KANN RASMUSSEN FONDEN

Louise Jivan Shah

Indholdsfortegnelse

Indholdsfortegnelse 5
Forskningsindhold.....7
Publikationer.....8
Foredrag 8
Anden formidling.....8
Regnskab.....9
Bilag 1: Artikel optaget i det videnskabelige tidsskrift Journal of Solar Energy Engineering, Transactions of the ASME. 10
Bilag 2: Artikel optaget i Proceedings for Energy-Efficient Building, Symposium in Sisimiut, Greenland.....28
Bilag 3: Artikel optaget i Installationsnyt - Specialhæfte nr. 46/2005. TechMedia A/S. 45
Bilag 4: Abstract accepteret til NorthSun 2005 Konferencen: Utilization of Solar Radiation at High Latitudes with Evacuated Tubular Collectors.....50
Bilag 5: Overheads til foredraget "*Evacuated Tubular Collectors*". 52
Bilag 6: Overheads/Poster til foredraget " *New Trnsys Model of Evacuated Tubular Collectors with Cylindrical Absorbers*". 69

Forskningsindhold

I projektets andet år har arbejdet bl.a. været koncentreret om undersøgelse og udvikling af teoretiske modeller til beregning af termiske ydelser for *Heat Pipe* vakuumrørsolfangere. *Heat Pipe vakuumrørsolfangere* består af en række cylinderformede glasrør som øverst er koblet til en kondensator/varmeveksler-enhed.
Inde i glasrørene med vakuum er placeret absorbere med selektiv belægning og et såkaldt heat pipe rør som indeholder et varmetransporterende medium, f.eks. vand. Det varmetransporterende medium fordamper ved et lavt temperaturniveau når absorberen opvarmes af solens stråler, idet der også er vakuum i heat pipe røret.
Dampen stiger opad i røret til en kondensator, hvor dampen kondenserer og derved afgiver varme til solfangervæsken, som pumpes gennem kondensator/varmeveksler-enheden. I kondensatoren kondenserer det varmetransporterende medium, der som væske flyder ned til bunden af røret hvor det igen fordamper hvis temperaturen er høj nok hvorefter processen gentages.

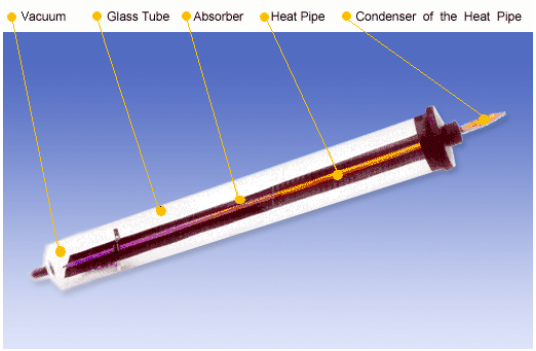

Fig. 1. Et Heat Pipe vakuumglasrør.

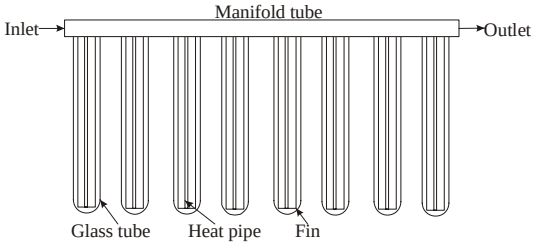

Fig. 2. Heat Pipe vakuumrørsolfangere.

Traditionelle solfangerteorier fra litteraturen er udviklet med henblik på almindelige plane solfangere med plane absorbere og har ikke kunnet benyttes direkte til Heat Pipe vakuumrørsolfangere. Derfor er der udviklet to nye teoretiske solfangermodeller til Heat Pipe vakuumrørsolfangere med hhv. krumme og plane finner. Modellerne udmærker sig især ved at de præcist bestemmer skyggeeffekterne fra rør til rør, ligesom de detaljeret bestemmer temperaturprofilet på finnen.

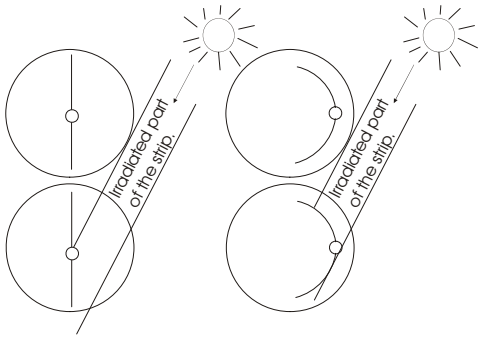

Fig. 3. Heat Pipe vakuumrør med hhv. plane og krumme finner.

Forberedelserne til det eksperimentelle arbejde er også godt i gang. En prøvestand til parallel afprøvning af forskelligt designede vakuumrørsolfangere er under opbygning. På baggrund af de indledende teoretiske undersøgelser er prototyper af forskelligt designede vakuumrørsolfangere udviklet i samarbejde med en kinesisk fabrikant, og disse solfangere skal side-by-side testes i løbet af de kommende måneder.

Med udgangspunkt i målingerne, teoretiske undersøgelser og økonomiske betragtninger vil veldesignede vakuumrørsolfangere blive identificeret i projektets tredje år.

Fig. 4. Prøvestand, til parallel afprøvning af forskelligt designede vakuumrørsolfangere, under opbygning.

Publikationer

Shah L.J., Furbo S. (2005)	*Modelling Shadows on Evacuated Tubular Collectors with Cylindrical Absorbers.* Journal of Solar Energy Engineering, Transactions of the ASME. In press.
Shah L.J. (2005)	*Evacuated Tubular Collectors.* Proceedings, Energy-Efficient Building, Vol. 1, pp.87-102. Symposium in Sisimiut, Greenland
Shah L.J., Furbo S. (2005)	*Utilization of Solar Radiation at High Latitudes with Evacuated Tubular Collectors.* Abstract accepted for the NorthSun 2005 Conference, Vilnius, Lithuania, May 25-27, 2005.
Shah L.J. (2005)	*Vakuumrørsolfangere til Arktis.* Installationsnyt - Specialhæfte nr. 46/2005. TechMedia A/S.

Foredrag

Shah L.J. (2005)	*Evacuated Tubular Collectors.* Energy-Efficient Building, Symposium in Sisimiut, Greenland, April 12-14 2005.
Shah L.J. (2004)	*New Trnsys Model of Evacuated Tubular Collectors with Cylindrical Absorbers.* EuroSun 2004 Congress, Freiburg, Germany, June 20-23, 2004.

Anden formidling

Undervisning bl.a. om vakuumrørsolfangere på Ph.D. kurset ”Solar Energy Systems”, Rigas Tekniske Universitet, Letland, 27. maj 2005.

Regnskab

Indbetalinger

Indtægter i alt

Forskertimer
Teknisk/adm. bistand
Rejser
Drift og materialer
Øvrige

Udgifter i alt

Saldo projektkonto

Kommentarer til regnskab:

Bilag 1: Artikel optaget i det videnskabelige tidsskrift Journal of Solar Energy Engineering, Transactions of the ASME.

MODELLING SHADOWS ON EVACUATED TUBULAR COLLECTORS WITH CYLINDRICAL ABSORBERS

Louise Jivan Shah & Simon Furbo
Department of Civil Engineering, Technical University of Denmark
Building 118
DK-2800 Kgs. Lyngby
Denmark
E-mail: ljs@byg.dtu.dk

Abstract

A new TRNSYS collector model for evacuated tubular collectors with tubular absorbers is developed. Traditional flat plate collector performance equations have been integrated over the whole absorber circumference. On each tube the model determines the size and position of the shadows caused by the neighbour tube.
An all glass tubular collector with tubular absorbers with 14 tubes connected in parallel is investigated theoretically with the model and experimentally in an outdoor collector test facility. Performance calculations with the new model are compared with measured results and a good degree of similarity between the measured and calculated results is found.
Further, it is illustrated how the model can be used for geometrical parameter studies both for constant collector mean fluid temperatures and for varying temperature conditions in a solar heating plant. These investigations are performed for two climates: Copenhagen (Denmark) and Uummannaq (Greenland).

Introduction

Evacuated tubular collectors (ETC) have an increasing share of the collector market in the world. Up to 2001 more than 100 million m² collectors were installed world over. Of this, about 28% were unglazed collectors, 49% were traditional flat plate collectors and about 22% were ETC [1].

As a consequence of this market development, almost all larger German and Austrian solar thermal companies have ETC on their product list. Due to the market development, also the theoretical modelling and simulation development becomes more and more important.

Of course, thermal modelling of evacuated tubular collectors has previously been addressed. Barrett A.L. et al [2] developed an evacuated tubular collector model that included two incidence angle modifiers for the longitudinal and the transverse direction. This model has widely been used, among others by, Qin L. and Furbo S. [3] who investigated the performance of differently designed evacuated solar collectors. The model cannot be used to find the efficiency expression and the incidence angle modifiers based on the tube geometry and panel design, since the model does not directly take into account shadow effects from adjacent tubes or solar radiation received from the back of the collector.

Perez et al [4] developed a radiation model for evacuated tubular collectors with tubular absorbers. The model was based on the theory of one-axis tracking solar collector and did take into account solar radiation received from the back of the collector. Further the model gave an estimation of the size of the shadowed area of the total collector panel. However, the model did not determine the position of the shadows on each tube.

Lart S. [5] found a geometrical method to determine the size and position of the shadowed area on each tube. This information was used to modify the transverse incidence angle modifier so that the effective absorber area was taken into account.

Shah, L.J. and Furbo, S. [6] worked further on this principle and developed a new ETC simulation model. The model was developed for ETC with tubular collectors mounted on ground in large collector fields. The advantages of the model were that shadows, the solar radiation and the incidence angle modifier for each tube were precisely determined for all solar positions, including solar positions on the "back" of the collector. However, the model could be improved further as the model was only valid for vertical pipes and as the model was not developed for a commonly used simulation program.

In the present paper, this theory is further developed so it can simulate solar collector panels of any tilt and based on the theory a new TRNSYS [7] collector type is developed. This model is validated with measurements from outdoor experiments.

Some examples of the model calculations of shadows on the tubes will be shown. Further, TRNSYS simulations of the yearly thermal performance of a solar heating plant based on the evacuated solar collectors are carried out and it is investigated how the distance between tubes and the collector tilt influences the yearly thermal performance.

Collector performance theory for tubular absorbers

In Shah, L.J. and Furbo, S [6,8], a theoretical model for calculating the thermal performance of ETC with tubular absorbers was developed. The principle in the model was that flat plate collector performance equations were integrated over the whole absorber circumference. In this way, the transverse incident angle modifier was eliminated. The model was valid only for vertically tilted pipes.

In this section, the principle of the model will shortly be summarized. Further, the newest development that improves the model to be able to also take tilted pipes into calculation will be described.

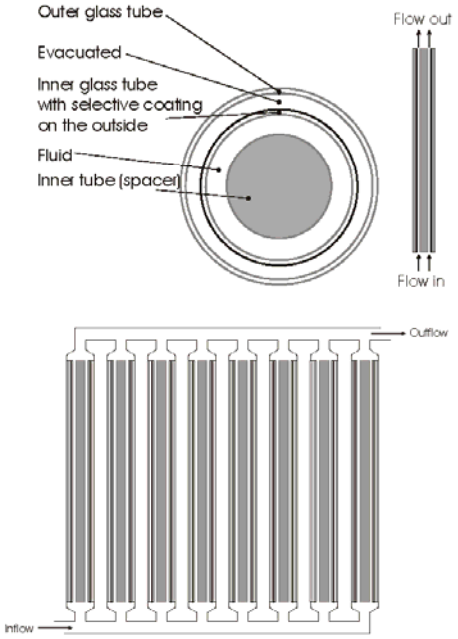

Fig. 1: Design of the evacuated tubes (top) and the tubes connected to a solar panel (bottom).

In principle, the theory is suitable for all ETC without reflectors. However, in this case, the theory development is based on a collector design with a number of parallel-connected double glass tubes, which are open in both ends. The tubes are annuluses with closed ends and the outside of the inner glass wall is equipped with an absorbing selective coating. The collector fluid is floating from bottom to top of the inside of the inner tube where also another closed tube is inserted with the purpose to fill out a part of the tube volume so that less collector fluid is needed. Further, it ensures a high heat transfer coefficient from the inner glass tube to the collector fluid. Figure 1 shows the design of the evacuated tubes and the tube connection.

Generally, for a solar collector without reflectors and without parts of the collector reflecting solar radiation to other parts of the collector, the performance equation can be written as:

$$P_u = P_b + P_d + P_{gr} - P_{loss} \quad (1)$$

or more detailed described:

$$P_u = A_b \cdot F' \cdot (\tau\alpha)_e \cdot K_\theta \cdot R_b \cdot G_b + A_a \cdot F' \cdot (\tau\alpha)_e \cdot K_{\theta,d} \cdot F_{c-s} \cdot G_d + A_a \cdot F' \cdot (\tau\alpha)_e \cdot K_{\theta,gr} \cdot F_{c-g} \cdot G_{gr} - A_a \cdot U_L \cdot (T_{fm} - T_a) \quad (2)$$

where K_θ is the incident angle modifier defined as [9]:

$$K_\theta = 1 - \tan^a\left(\frac{\theta}{2}\right) \quad (3)$$

The incident angle modifiers for diffuse radiation, $K_{\theta,d}$, and ground reflected radiation, $K_{\theta,gr}$, are evaluated by Eq. 3 using $\theta=\pi/3$.

To calculate the thermal performance of the evacuated tubes, the general performance Eq. (1) and Eq. (2) have been integrated over the whole absorber circumference. This means that the tube is divided into small "slices", and each slice is treated as if it was a flat plate collector. In this way, the transverse incident angle modifier is eliminated. To describe the solar radiation on a tubular geometry, this method has previously been used by Pyrko J. [10].

Integrating over the absorber area, the performance equation can be described as:

$$P_u = \int_{-\pi}^{\pi} \left(P_b + P_d + P_{gr} - P_{loss}\right) \cdot d\xi \tag{4}$$

where,

$$P_{loss} = \int_{-\pi}^{\pi} A_a \cdot U_L \cdot (T_{fm} - T_a) \cdot d\xi \quad = \int_{-\pi}^{\pi} L \cdot r_p \cdot U_L \cdot (T_{fm} - T_a) \cdot d\xi \quad = 2 \cdot \pi \cdot L \cdot r_p \cdot U_L \cdot (T_{fm} - T_a) \tag{5}$$

$$P_d = \int_{-\pi}^{\pi} A_a \cdot F' \cdot (\tau\alpha)_e \cdot K_{\theta,d} \cdot F_{c-s} \cdot G_d \cdot d\xi \quad = 2 \cdot \pi \cdot r_p \cdot L \cdot F' \cdot (\tau\alpha)_e \cdot K_{\theta,d} \cdot G_d \cdot \int_{-\pi}^{\pi} F_{c-s} \cdot d\xi \tag{6}$$

$$P_{gr} = \int_{-\pi}^{\pi} A_a \cdot F' \cdot (\tau\alpha)_e \cdot K_{\theta,gr} \cdot F_{c-g} \cdot G_{gr} \cdot d\xi \quad = 2 \cdot \pi \cdot r_p \cdot L \cdot F' \cdot (\tau\alpha)_e \cdot K_{\theta,gr} \cdot G_{gr} \cdot \int_{-\pi}^{\pi} F_{c-g} \cdot d\xi \tag{7}$$

$$G_{gr} = \rho_{gr} \cdot (G_b + G_d) \tag{8}$$

$$F_{c-s} = 0.5 - F_{1-2} \tag{9}$$

$$F_{c-g} = 0.5 - F_{1-2} \tag{10}$$

Power from beam radiation on collector/tube, P_b:

The power contribution from the beam radiation can be written as:

$$\begin{aligned} &0 < \gamma_1 - \gamma_0 \le \pi: \quad P_b = \int_{\gamma_0}^{\gamma_1} F' \cdot (\tau\alpha)_e \cdot G_b \cdot A_b \cdot K_\theta \cdot R_b \cdot d\xi \quad = F' \cdot (\tau\alpha)_e \cdot G_b \cdot L \cdot r_p \cdot \int_{\gamma_0}^{\gamma_1} K_\theta \cdot R_b \cdot d\xi \\ &0 \le \gamma_0 - \gamma_1 < \pi: \quad P_b = \int_{\gamma_1}^{\gamma_0} F' \cdot (\tau\alpha)_e \cdot G_b \cdot A_b \cdot K_\theta \cdot R_b \cdot d\xi \quad = F' \cdot (\tau\alpha)_e \cdot G_b \cdot L \cdot r_p \cdot \int_{\gamma_1}^{\gamma_0} K_\theta \cdot R_b \cdot d\xi \end{aligned} \tag{11}$$

Notice that there is now integrated over only a part of the circumference. This is because only part of the absorber surface is exposed to the beam radiation due to shadows from the neighbour tube. The task is now to determine the size of this area, thus determining the size and position of the shadowed area. In vector notation, the position of the sun can be described by:

$$\vec{S} = \begin{pmatrix} \sin\theta_z \cdot \cos\gamma_s \\ \sin\theta_z \cdot \sin\gamma_s \\ \cos\theta_z \end{pmatrix} \quad (12)$$

and a "cross section circle" (see Fig. 2) on the absorber of one tube can be described by:

$$\vec{N} = r_p \cdot \begin{pmatrix} \cos\left(\frac{\pi}{2} - \beta_s\right) \cdot \cos\gamma_0 \\ \sin\gamma_s \\ \sin\left(\frac{\pi}{2} - \beta_s\right) \cdot \sin\gamma_0 \end{pmatrix} \quad (13)$$

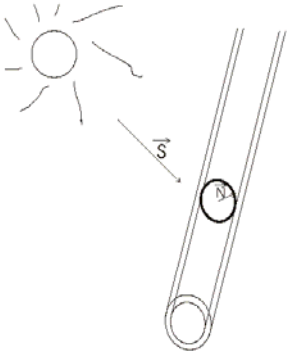

Fig. 2: The solar vector, $\vec{S}$, and the tube vector, $\vec{N}$.

Figure 3 shows an example where a part of one tube is shaded and a part is exposed to beam radiation. In order to determine the size of the area exposed to beam radiation, the points P_0 and P_1 must be determined.

Since P_0 is located where the solar vector and the tube vector are at right angles to each other, P_0, described by the angle γ_0, can be determined by the scalar product of the two vectors:

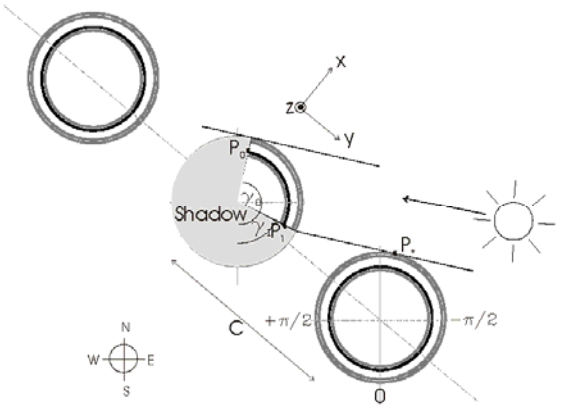

Fig. 3: Illustration of the shaded area and the area exposed to beam radiation.

$$\vec{S} \cdot \vec{N} = |S| \cdot |N| \cdot \cos\left(\frac{\pi}{2}\right) = 0 \Rightarrow \sin\theta_z \cdot \cos\gamma_s \cdot \cos\left(\frac{\pi}{2} - \beta_s\right) \cdot \cos\gamma_0 + \sin\theta_z \cdot \sin\gamma_s \cdot \sin\gamma_0 + \cos\theta_z \cdot \sin\left(\frac{\pi}{2} - \beta_s\right) \cdot \sin\gamma_0 = 0 \Rightarrow$$

$$\gamma_0 = -\arctan\left(\frac{\sin(\theta_z) \cdot \cos(\gamma_s) \cdot \cos(\frac{\pi}{2} - \beta_s) + \cos(\theta_z) \cdot \sin(\frac{\pi}{2} - \beta_s)}{\sin(\theta_z) \cdot \sin(\gamma_s)}\right) \quad (14)$$

Since the equation for γ_0 involves the arctan function, the equation will return two solutions. Based on information on the position of the sun, the correct solution is found.

The point P_1, described by the angle γ_1, can be determined from the following Eq. (15), (16) and (17). A graphical illustration of symbols used in the equations can be seen in Fig. 3 and Fig. 4.

$$P_1 = \begin{pmatrix} x_1 \\ y_1 \\ z_1 \end{pmatrix} = \begin{pmatrix} x_* \\ y_* \\ z_* \end{pmatrix} + \begin{pmatrix} \sin\theta_z \cdot \cos\gamma_s \\ \sin\theta_z \cdot \sin\gamma_s \\ \cos\theta_z \end{pmatrix} \cdot T \qquad (15)$$

$$P_1 = \begin{pmatrix} x_1 \\ y_1 \\ z_1 \end{pmatrix} = \begin{pmatrix} x_n \\ 0 \\ z_n \end{pmatrix} + r_p \cdot \begin{pmatrix} \cos\left(\frac{\pi}{2} - \beta_s\right) \cdot \cos\gamma_1 \\ \sin\gamma_1 \\ \sin\left(\frac{\pi}{2} - \beta_s\right) \cdot \sin\gamma_1 \end{pmatrix} \qquad (16)$$

$$x_n = -z_n \cdot \tan\left(\frac{\pi}{2} - \beta_s\right) \qquad (17)$$

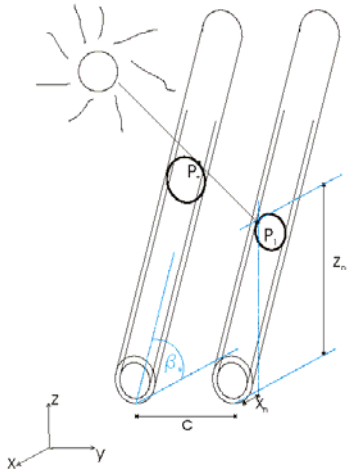

Fig. 4: Illustration of the beam radiation passing one tube and hitting the next tube..

Equations (15) (16) and (17) together give four equations to the four unknowns: T, γ_1, x_n and z_n. Solving for γ_1 gives:

$$\gamma_1 = \arctan 2\left[\frac{K_1 + 0.5 \cdot \frac{K_2}{K_2^2 + K_3^2} \cdot \left(-2 \cdot K_1 \cdot K_2 + 2 \cdot K_4^{0.5}\right)}{K_3}, \frac{0.5}{K_2^2 + K_3^2} \cdot \left(-2 \cdot K_1 \cdot K_2 + 2 \cdot K_4^{0.5}\right)\right]$$

or (18)

$$\gamma_1 = \arctan 2\left[\frac{K_1 + 0.5 \cdot \frac{K_2}{K_2^2 + K_3^2} \cdot \left(-2 \cdot K_1 \cdot K_2 - 2 \cdot K_4^{0.5}\right)}{K_3}, \frac{0.5}{K_2^2 + K_3^2} \cdot \left(-2 \cdot K_1 \cdot K_2 - 2 \cdot K_4^{0.5}\right)\right]$$

where arctan2(X,Y) is defined as tan(Y/X) and

$$K_1 = \frac{x_*}{\tan\left(\frac{\pi}{2} - \beta_s\right)} - \frac{y_*}{\tan\left(\frac{\pi}{2} - \beta_s\right) \cdot \tan(\gamma_s - \gamma_f)} - \frac{y_*}{\tan(\theta_z) \cdot \sin(\gamma_s - \gamma_f)} + z_*$$

$$K_2 = \frac{C}{\tan\left(\frac{\pi}{2} - \beta_s\right) \cdot \tan(\gamma_s - \gamma_f)} + \frac{C}{\tan(\theta_z) \cdot \sin(\gamma_s - \gamma_f)} \qquad (19)$$

$$K_3 = C \cdot \left(\cos^2\left(\frac{\pi}{2} - \beta_s\right) + \frac{1}{\tan(\theta_z) \cdot \sin(\gamma_s - \gamma_f)}\right)$$

$$K_4 = K_3^4 - K_1^2 \cdot K_3^2 + K_2^2 \cdot K_3^2$$

From Eq. (18) it appears that there are two solutions for γ_1. Based on information on the position of γ_0, the correct solution is found.

The incident angle, θ, and the geometric factor, R_b:

The incident angle, θ, can be described as:

$$\cos(\theta) = \sin(\theta_z)\cdot\cos(\gamma_s - \gamma_f)\cdot\cos\left(\frac{\pi}{2} - \beta_s\right)\cdot\cos(\gamma_{actual}) + \sin(\theta_z)\cdot\sin(\gamma_s - \gamma_f)\cdot\sin(\gamma_{actual}) + \cos(\theta_z)\cdot\sin\left(\frac{\pi}{2} - \beta_s\right)\cdot\cos(\gamma_{actual}) \quad (20)$$

The geometric factor, R_b, can be described as [11]:

$$R_b = \frac{\cos(\theta)}{\cos(\theta_{zl})} \quad (21)$$

Solving the performance equation:

In order to evaluate the performance of the tubular collector on a yearly basis, the above theory is implemented into a Trnsys type. All the integrals can be solved analytically, except the integral in Eq. (11), which is solved by using the trapezoidal formula for solving integrals numerically. 360 integration steps are used in the numerical integration. Taking the collector capacity into account, the collector outlet temperature is evaluated by:

$$P_u = \dot{V}\cdot\rho\cdot C_p\cdot\left(T_{out,hot} - T_{in,cold}\right) + \frac{C_{p,col}\cdot(T_{fm}^{t} - T_{fm}^{t-\Delta t})}{\Delta t} \quad (22)$$

Measurements and model validation

The model was validated with a prototype collector based on the collector principle shown in Fig. 1. Data of the collector is given in Table 1 and a photo of the collector is shown in Fig. 5.

No. of pipes	[-]	14
L	[m]	1.47
r_c	[m]	0.0235
r_p	[m]	0.0185
C	[m]	0.067
k_{tube}	[W/m²K]	0.8
$k_{manifold}$	[W/K/(m manifold)]	0.134
F'	[-]	0.98
$(\tau\alpha)_e$	[-]	0.856
a	[-]	3.8
$C_{collector}$	[kJ/K/tube]	1.9

Table 1: Data describing the collector in the model.

The thermal performance of the collector was measured in an outdoor test facility where the inlet temperature, the outlet temperature and the volume flow rate was measured. The temperatures were measured with copper-constantan thermocouples (Type TT) and the volume flow rate was measured with a HGQ1 flow meter. A 31% glycol/water mixture was used in the solar collector loop. Further, the global radiation and the diffuse radiation on horizontal were measured with two Kipp&Zonen CM5 pyranometers.

The collector performance was measured for two different tilts: 45° and 90° (both facing south). A period of 11 days (17/5-28/5 2003) has been selected for validating the Trnsys model for the collector at 45° and a period of 7 days (12/8-19/8 2003) has been selected for validating the Trnsys model for the collector at 90°.

The necessary data for describing the collector are shown in Table 1. The heat loss coefficient, k_0, was determined from efficiency measurements [6] and split into two parts for the evacuated tubes and the manifold pipes respectively. F' was calculated from theory [11,12] and $(\tau\alpha)_e$ and *a* were calculated with a simulation program for determining optical properties [13].

Fig. 5: Photo of the tested collector.

In Fig. 6 the measured and calculated collector outlet temperatures are compared. It can be seen that there is a good degree of similarity between the measured and calculated temperatures. The difference between measured and calculated outlet temperature, dT, is always close to 0 K and the maximum temperature difference is about 3 K.
Further Fig. 7 shows the measured and calculated collector performance for the two periods. The difference between the measured and calculated performance lies within the measuring inaccuracy of 4%.

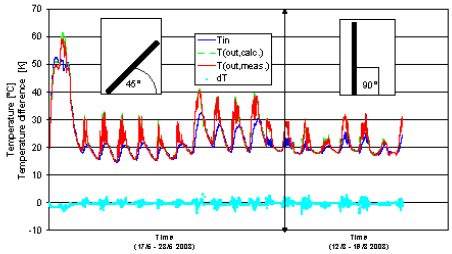

Fig. 6: Measured and calculated outlet temperature for the test periods

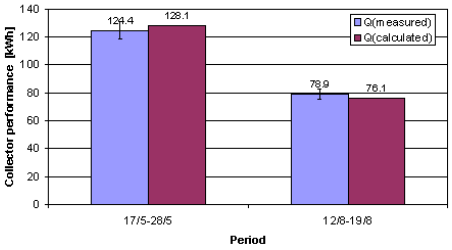

Fig. 7: Measured and calculated collector performance for the test periods.

Calculation of the tube area exposed to beam radiation

One of the features of the new model is that it determines the tube area exposed to beam radiation. This area corresponds to the size of the angle of the non-grey area on the middle pipe illustrated in Fig. 3.

For illustration purpose, Fig. 8 shows the angle on the tube exposed to beam radiation as a function of the solar azimuth and zenith, when the centre tube distance is 0.067 m, the outer tube radius is 0.0235 m and the inner tube radius is 0.0185 m.

Each sub-figure in Fig. 8 shows the angle exposed to beam radiation for a constant solar zenith, and each sub-figure contains six curves that represent different tube tilts from 0° to 75°. If one of these curves shows that the angle exposed to beam radiation is 180°, it means that there is no shadow from the adjacent tubes. Likewise, if one of these curves shows that the angle exposed to beam radiation is 0°, it means that there is full shadow from the adjacent tubes.

As expected, Fig. 8 shows that the smaller the zenith the larger the angle exposed to beam radiation. Also the figure shows that for small zenith angles, small tube tilts are preferable and vice versa.

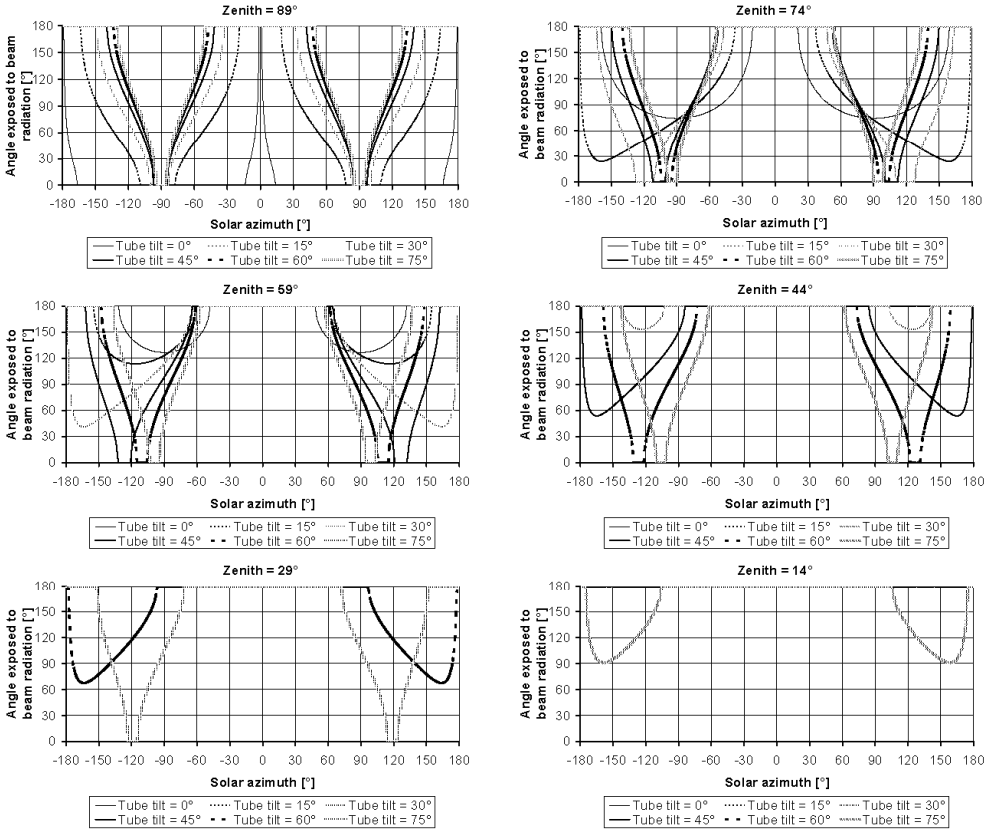

Fig. 8: The angle on the tube exposed to beam radiation as a function of the solar azimuth and zenith, when the centre tube distance is 0.067 m.

To show the influence of the tube centre distance, Fig. 9 shows the angle on the tube exposed to beam radiation as a function of the solar azimuth and zenith, when the centre tube distance is now 0.047 m. This means that there is no air gap between the tubes. The outer and inner tube radiuses are still 0.0235 m and 0.0185 m.

Comparing Fig. 8 and Fig. 9 it becomes clear that the smaller the tube centre distance is the more shadow will come from the adjacent tubes. This is especially clear for the smallest zeniths. For example for a zenith of 29° there are only shadows on the tubes tilted 60° and 75° when the tube centre distance is 0.067m whereas for a tube centre distance of 0.047m there are shadow on all the tilted tubes.

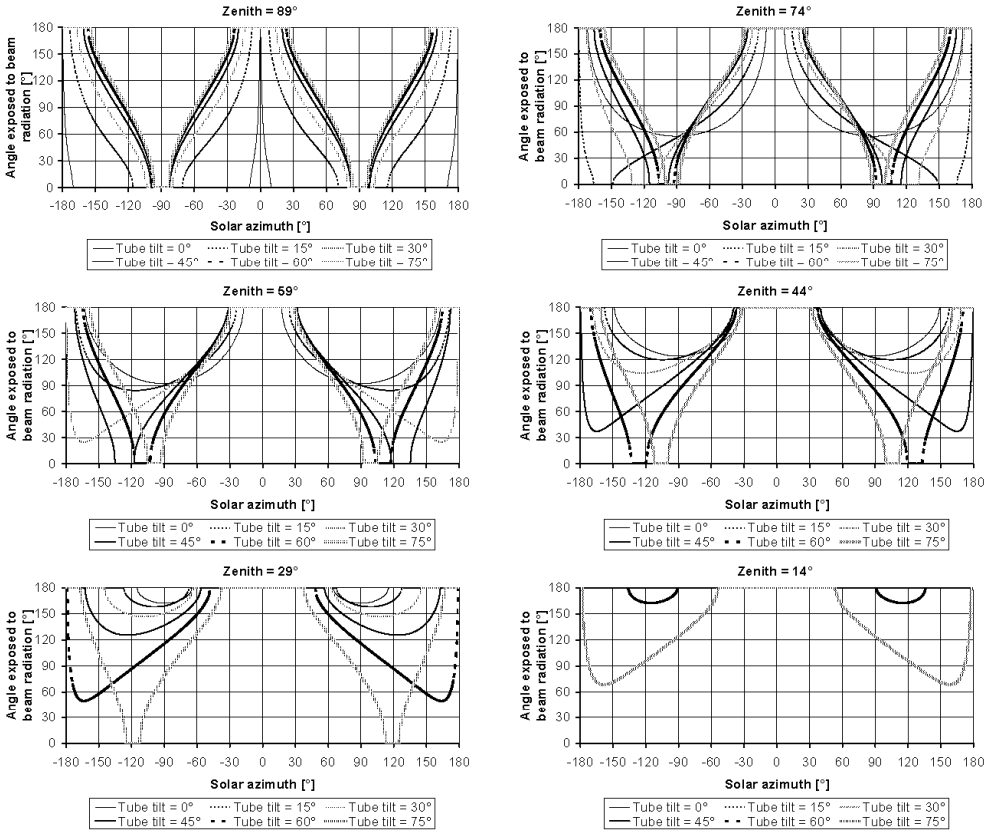

Fig. 9: The angle on the tube exposed to beam radiation as a function of the solar azimuth and zenith, when the centre tube distance is 0.047 m.

Parameter variations

In this section, it is illustrated how the model can be used for geometrical parameter studies. In the following examples it is assumed that the ETC collector panel is operating in a solar heating plant at a constant temperature of 50°C throughout the year. The model data of the collector panel is given in Table 1. The collector performance is investigated for two climates, as summarized in Table 2. The albedo is set higher for Uummannaq during a large part of the year due to snow on the ground.

Location	Latitude [°]	Longitude [°]	$T_{a,average}$ [°C]	G_{global} [kWh/m²]	$G_{diffuse}$ [kWh/m²]	Albedo [-]	Reference
Copenhagen, Denmark	56	12	7.8	1002	510	0.2	[14]
Uummannaq, Greenland	71	52	-4.2	888	409	0.2 (15/6-14/9) 0.7 (15/9-14/6)	[15]

Table 2: Summarized data for the two locations.

The following parameters are analysed:

- Collector tilt and collector azimuth (geometry unchanged)
- Inner tube radius (outer tube radius constant)
- Tube centre distance (tilt and orientation unchanged)

Figure 10 shows the thermal performance per tube for Copenhagen and Uummannaq respectively. The figure clearly shows how the thermal performance decreases when the collector orientation deviates from south. The figure also shows that the optimum tilt is about 45° for Copenhagen and about 60° for Uummannaq.

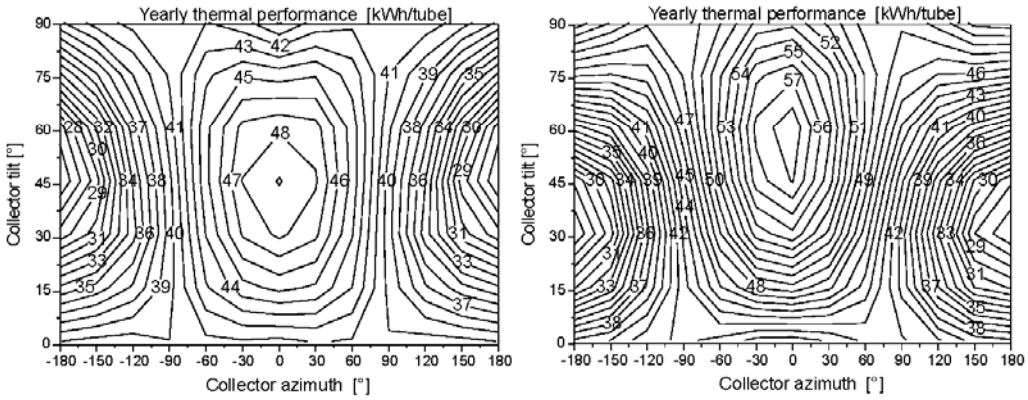

Fig. 10: The thermal performance per tube, at a fluid mean temperature of 50°C, as a function of the collector tilt and orientation for Copenhagen (Left) and Uummannaq (Right).

Figure 11 shows the thermal performance per tube as a function of the inner tube radius for a collector fluid temperature of 50°C. The outer tube radius is kept constant 0.0235 m and the tube heat loss coefficient is assumed to vary linear with the absorber area. The figure shows that the thermal performance increases with the inner tube radius. The increase is not linear as the heat loss coefficient also increases with increasing inner tube radius.

For both locations, Fig. 12 shows the thermal performance per tube as a function of the tube centre distance for different collector fluid temperatures. The thermal performance increases for increasing tube centre distances up to a certain level, due to reduced shaded areas. For even larger distances the utilized energy decreases again, due to the

increasing heat loss from the manifold pipes. The optimal tube centre distance differs for different collector fluid temperatures. For a temperature of 70°C, the optimal tube centre distance is about 0.15 m and for a temperature level 30°C, the optimal tube centre distance is about 0.3 m. For higher temperature levels the heat losses from the manifold pipes becomes more important, and this explains the differences in the optimal tube centre distances.

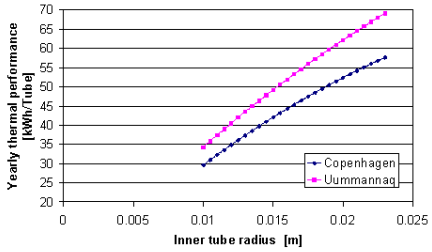

Fig. 11: The thermal performance per tube as a function of the inner tube radius for a collector fluid mean temperature of 50°C.

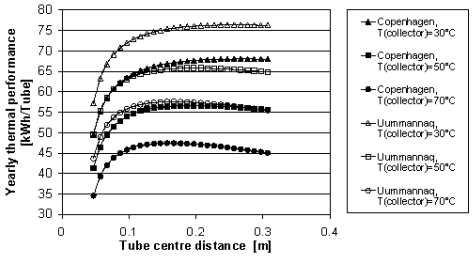

Fig. 12: The thermal performance per tube as a function of the tube centre distance for different collector fluid mean temperatures.

Simulation of solar heating plants

Model description

To illustrate simulation examples when the collector fluid mean temperature is not constant throughout the year, a model of a solar heating plant is built in TRNSYS.

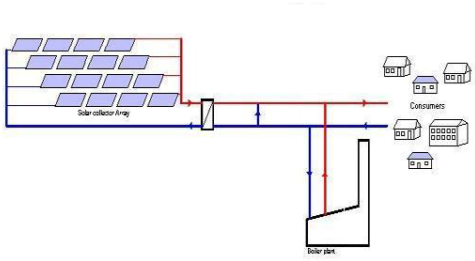

Fig. 13: Schematic illustration of the TRNSYS model.

The collector array consists of 100 rows where the distance between the rows is assumed to be so large that the shadows between the rows have negligible influence on the collector performance. The energy consumption of a town is defined by a water mass flow rate, a return temperature and a flow temperature of 80°C. If the temperature from the solar heat exchanger is above 80°C the temperature is mixed down to 80°C with at three-way valve.

If the temperature from the solar heat exchanger is below 80°C, an auxiliary boiler plant heats up the district heating water to 80°C.
An illustration of the TRNSYS model can be seen in Fig. 13 and Fig. 14 shows the mass flow rate and a flow and return temperature through out the year for the district heating net of the town. The annual heat consumption of the town is about 32500 MWh.

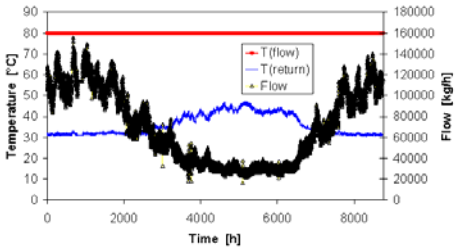

Fig. 14: Assumed flow rate and temperatures in the district heating net.

Tube distance, collector tilt and collector orientation

The optimum tube centre distance, collector tilt and orientation with respect the thermal performance per tube is investigated for the two locations. The gross collector area is assumed to be constant in the solar heating plant. Consequently, there are more tubes in the collector area when the tube distance is small than when the tube distance is large. Table 3 shows how the collector orientation, the tilt and the tube distance are varied.

Collector azimuth [°]	-90 (east), 75, 60, 45, 30, 15, 0, 15, 30, 45, 60, 75, 90 (west)
Collector tilt [°]	15, 30, 45, 60, 75, 89
Tube centre distance [m]	0.048, 0.107, 0.167, 0.227, 0.287, 0.347 (corresponds to 1mm – 300 mm of air gap between the tubes)

Table 3: Overview of the parameter variations performed with the model.

Figure 15 and Fig. 16 show the thermal performance per tube for Copenhagen and Uummannaq respectively. The figures clearly show how the thermal performance increases with increasing tube centre distances up to about 0.3 m for Copenhagen and 0.27 m for Uummannaq. The increase is caused by less shadow from the adjacent tubes. Further, the temperature level in the collectors is increased with decreasing tube centre distances as there totally are more tubes in the collector field and this temperature increase also decreases the thermal output per tube.

The figures also show that the optimum tilt and orientation is about 45° south for Copenhagen and about 60° south for Uummannaq.

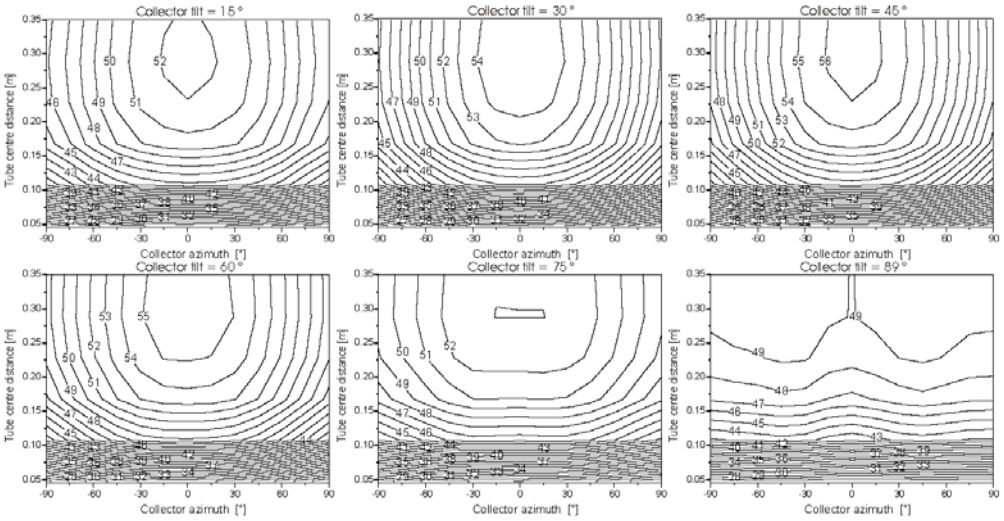

Fig. 15: The thermal performance per tube [kWh/Tube/Year] as a function of the tube centre distance, collector tilt and orientation (Copenhagen).

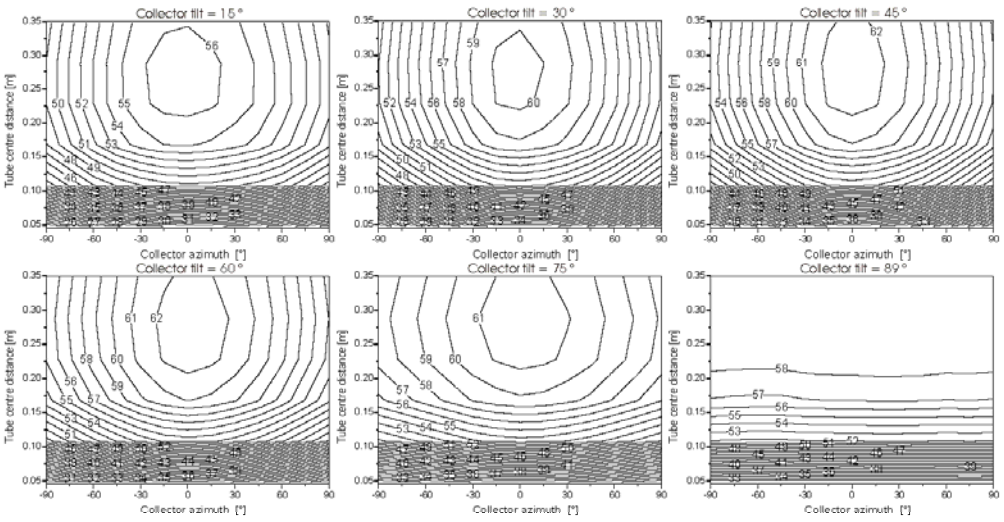

Fig. 16: The thermal performance per tube [kWh/Tube/Year] as a function of the tube centre distance, collector tilt and orientation (Uummannaq).

Conclusions

A new TRNSYS collector model for evacuated tubular collectors with tubular absorbers is developed. The model is based on traditional flat plate collector theory, where the

performance equations have been integrated over the whole absorber circumference. On each tube the model determines the size and position of the shadows caused by the neighbour tube as a function of the solar azimuth and zenith. This makes it possible to calculate the energy from the beam radiation.

The thermal performance of an all glass tubular collector with 14 tubes connected in parallel is investigated theoretically with the model and experimentally in an outdoor collector test facility. Calculations with the new model of the tubular collector vertically placed and tilted 45° is compared with measured results and a good degree of similarity between the measured and calculated results is found.

For two climates Copenhagen (Denmark) and Uummannaq (Greenland), it is illustrated how the model can be used for geometrical parameter studies.

For constant collector mean fluid temperature conditions throughout the year, the influence on the yearly thermal performance of the tube centre distance and the inner tube radius is investigated. These results show that to achieve the highest thermal performance, the tube centre distance must be about 0.2 m, and the inner tube radius should be as large as possible.

Also, the collector model is used in a model of a solar heating plant with varying temperatures and a sensitivity analysis of the tube centre distance, collector tilt and orientation with respect to the yearly thermal performance per tube is made. For the investigated load, the results show that the optimum tilt and orientation is about 45° south for Copenhagen and about 60° south for Uummannaq. These optima are not influenced by the average temperature level of the collectors.

References

[1]	Weiss W., Bergmann I, Faninger G. (2004). *Solar Heating Worldwide. Markets and Contributions to the Energy Supply 2001.* IEA Solar Heating & Cooling Programme, Feb. 2004.
[2]	Barrett A.L. et al (1988) *Thermal modelling of evacuated tubular solar collectors.* Solar 88, Proceedings of the 1988 annual meeting of the American Solar Energy Society. pp 505-510.
[3]	Qin L. and Furbo S. (1999) *Evaluation of Evacuated Tubular Solar Collectors for Large SDHW Systems and Combined Space Heating Systems.* Proceedings of NorthSun99, August 11-14, 1999, Edmonton, Alberta, Canada
[4]	Perez et al (1995) *Calculating solar radiation received by tubular solar energy collectors.* Solar Engineering, Vol. I, pp. 699-704.
[5]	Lart S. (2000) *Development of a thermal performance test for an Integrated Collector-Storage solar water heating system.* pp. 90-100. Ph.D. thesis. Division of Mechanical Engineering and Energy studies. University of Wales Cardiff.
[6]	Shah, L.J. and Furbo, S. (2004). *Vertical evacuated tubular collectors utilizing solar radiation from all directions.* Applied Energy, Vol 78/4 pp 371-395.
[7]	Klein, S.A. et al (1996). TRNSYS 14.2, User Manual. University of Wisconsin Solar

	Energy Laboratory.
[8]	Shah, L.J. and Furbo, S. (2003). *Thermal performance of evacuated tubular collectors utilizing solar radiation from all directions*. Proceedings, ISES World Sun Congress, Gothenburg
[9]	Gordon J. (ed.) (2001). *Solar Energy. The State of the Art. ISES Position papers.* James & James, London. ISBN: 1-902916-23-9.
[10]	Pyrko J. (1984). *A model of the average solar radiation for the tubular collector.* Int. J. Solar Energy. Vol. 32, pp. 563-565.
[11]	Duffie J.A. and Beckman W.A. (1991). *Solar Engineering of Thermal Processes*, 2nd edn. Wiley Interscience, New York.
[12]	Incropera F.P. and de Witt D.P. (1990). *Introduction to heat transfer*, pp. 428-467, John Wiley & Sons, Singapore.
[13]	Svendsen S. and Jensen F.F. (1994). *Soltransmittans.* Lecture note. Thermal Insulation Laboratory, Technical University of Denmark.
[14]	Lund H. (1995). *The Design Reference Year user manual.* Report of IEA-SHC Task 9. Report 274. Thermal Insulation Laboratory. Technical University of Denmark.
[15]	Kragh J. et al (2002). *Grønlandske vejrdata. Nuuk. Uummannaq*. Department of Civil Engineering, Technical University of Denmark . November 2002.

Acknowledgement

This study is financed by the VILLUM KANN RASMUSSEN FOUNDATION.

Nomenclature

LATIN SYMBOLS:

a	Incident angle modifier constant	[-]
A_a	Absorber area	[m²]
A_b	Absorber area exposed to beam radiation	[m²]
C	Tube centre distance	[m]
C_p	Collector fluid heat capacity	[J/(kg·K)]
$C_{collector}$	Collector panel heat capacity incl. fluid	[kJ/K/Tube)]
F'	Collector efficiency factor	[-]
F_{1-2}	View factor from tube 1 to tube 2	[-]
F_{c-g}	View factor from tube to ground	[-]
F_{c-s}	View factor from tube to sky	[-]
G_b	Beam radiation on horizontal	[W/m²]
G_d	Diffuse radiation on horizontal	[W/m²]
G_{gr}	Ground reflected radiation on horizontal	[W/m²]
k_{tube}	Heat loss coefficient per tube with respect to the absorber area	[W/m²K]
$k_{manifold}$	Manifold heat loss coefficient per meter manifold pipe	[W/mK]
K_1	Help variable	[-]
K_2	Help variable	[-]
K_3	Help variable	[-]
K_4	Help variable	[-]
K_θ	Incident angle modifier for beam radiation	[-]
$K_{\theta,d}$	Incident angle modifier for diffuse radiation	[-]
$K_{\theta,gr}$	Incident angle modifier for ground reflected radiation	[-]
$\vec{N}$	Tube vector	[-]
N	Number of tubes	[-]
L	Pipe length	[m]
P_b	Energy from beam radiation on collector/tube	[W]
P_d	Energy from diffuse radiation on collector/tube	[W]
P_{gr}	Energy from ground reflected radiation on collector/tube	[W]
P_{loss}	Heat loss from collector/tube	[W]
P_u	Useful energy from collector/tube	[W]
$Q_{auxiliar}$	Energy supplied from the boiler plant	[kWh]
Q_{town}	Energy supplied to the town	[kWh]
R_b	Geometric factor; irradiance on a tilted surface divided by irradiance on a horizontal surface	[-]

r_c	Outer glass tube radius	[m]
r_p	Absorber radius	[m]
$\vec{s}$	Solar vector	[-]
T_a	Ambient temperature	[°C]
T_{fm}	Fluid mean temperature	[°C]
$T_{in,hot}$	Hot inlet temperature	[°C]
$T_{out,cold}$	Cold outlet temperature	[°C]
T	Help parameter	[-]
U_L	Heat loss coefficient based on absorber area	[W/(m²K)]
$\dot{V}$	Collector volume flow rate	[m³/s]
x_1	x coordinate for P_1	[m]
x_n	Help length	[m]
x_*	x coordinate for P_*	[m]
y_1	y coordinate for P_1	[m]
y_*	y coordinate for P_*	[m]
z_1	z coordinate for P_1	[m]
z_n	Help length	[m]
z_*	z coordinate for P_*	[m]

GREEK SYMBOLS:

β_s	Collector panel tilt	[rad]
γ_s	Solar azimuth	[rad]
ρ	Collector fluid density	[kg/m³]
θ	Incident angle	[rad]
θ_z	Solar zenith	[rad]
$\tau\alpha_e$	Effective transmittance-absorptance product	[-]
ξ	Integration variable	[rad]
γ_0	Integration border	[rad]
γ_1	Integration border	[rad]
γ_f	Collector panel azimuth	[rad]
γ_{actual}	Actual absorber azimuth	[rad]

Bilag 2: Artikel optaget i Proceedings for Energy-Efficient Building, Symposium in Sisimiut, Greenland

Evacuated Tubular Collectors

Louise Jivan Shah, Assoc. Professor, Department of Civil Engineering Technical University of Denmark, ljs@byg.dtu.dk

ABSTRACT
In this paper two research examples on evacuated tubular collectors are given. The first example concerns development of theoretical models for Heat pipe evacuated tubular collectors. In the second example heat transfer and flow structures inside All-glass evacuated tubular collectors for different operating conditions are investigated by means of Computational Fluid Dynamics (CFD).

1 INTRODUCTION

Solar energy is a clean and natural energy source. The solar radiation on earth – including at Arctic latitudes – is so large that it is possible to utilize solar energy in large scale.
The yearly *number of hours* with possibility of sunshine is almost independent of the latitude. However, Fig. 1 and Fig. 2 show that the distribution of the solar radiation on a monthly basis strongly depends on the latitude. At northern latitudes:

- more solar radiation occurs during the summer months
- the sun altitude is lower
- the day length variation is larger

For example, north of the Arctic Circle in the summer the sun is present 24 hours a day and solar radiation occurs from all directions during the 24 hours.

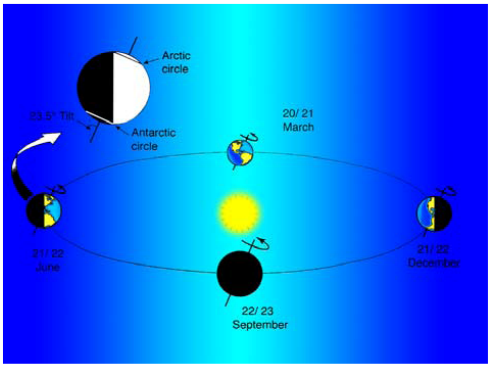

Fig. 1: The earth's path around the sun.

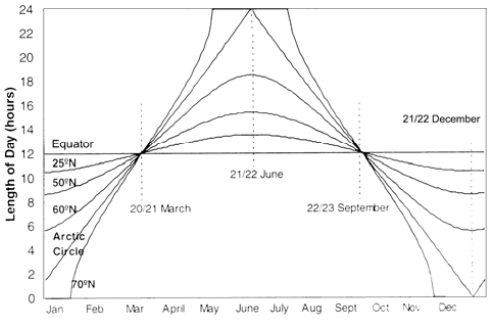

Fig. 2: The day length as a function of latitude and the season.

1.1 Evacuated tubular collectors

When solar collectors are developed for Arctic conditions, it is an advantage if the collector design can utilize solar radiation from all directions. Due to low ambient temperatures it is also an advantage if the collector has a low heat loss so that as little as possible of the absorbed solar radiation is lost to the surroundings. Further, the collector must be able to utilize ground reflected radiation, as the snow on the ground has a large reflection coefficient. Evacuated tubular collectors can be designed to fulfil these demands. Basically there exist two types of evacuated tubular collectors:

Heat pipe evacuated tubular collectors consist of cylindrical evacuated glass tubes which are connected to a condenser/heat exchanger unit. Inside the evacuated tubes are the absorber fins with selective coatings on the surfaces and with a heat pipe, which contains the working fluid, for example water. The working fluid evaporates at a low temperature when the absorber is heated by the solar radiation. The evaporated fluid rises in the pipe and condenses on the condenser in the heat exchanger unit. Thus the energy is transferred to the solar collector fluid, which is pumped through the condenser/heat exchanger unit. When the working fluid in the heat pipe condenses, it drops down in the heat pipe again and the whole process is repeated if the temperature is high enough. Fig. 3 shows an evacuated glass tube with a heat pipe.

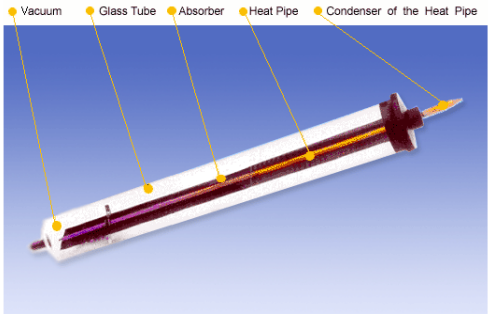

Fig. 3: An evacuated glass tube with a heat pipe.

All-glass evacuated tubular collectors are designed in a different way. They are based on double glass tubes (see Fig. 4) with the evacuated space between the glass tubes. The outside of the inner glass wall is treated with an absorbing selective coating and works as the absorber. With solar irradiation on the tube, the inner glass tube gets very hot. The heat can be transferred from the inner glass tube to the solar collector fluid in different ways: Either the solar collector fluid is flowing directly inside the inner glass tube or the solar collector fluid can flow in a metal pipe, which is in good thermal contact with the inner glass tube.

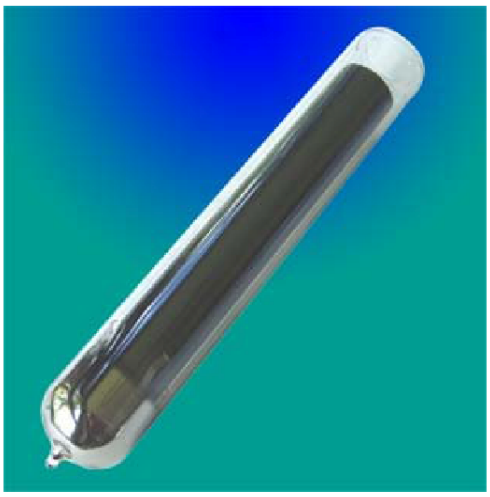
Fig. 4: A double glass tube.

Evacuated tubular collectors are suitable for Arctic conditions as:

- The collectors have a low heat loss coefficient. Due the evacuated space in both types of evacuated tubular collectors, the heat loss due to convection and conduction is very small. Therefore, the heat loss from evacuated tubular collectors is lower than the heat loss from traditional flat plate collectors.
- The collectors can utilize solar radiation from all directions. All-glass evacuated tubular collectors have cylindrical absorbers and in Heat pipe evacuated tubular collectors the absorber fin can have a curved shape, which follows the shape of the glass tube.
- The curved/cylindrical absorber shape can further utilize the ground reflected radiation better.

In order to develop optimum designed evacuated tubular collectors for Arctic conditions detailed background research is needed. In chapter 2 and 3 two research examples are given. The first example concerns development of theoretical models for Heat pipe evacuated

tubular collectors. In the second example heat transfer and flow structures inside All-glass evacuated tubular collectors for different operating conditions are investigated by means of Computational Fluid Dynamics (CFD).

2 RESEARCH EXAMPLE 1: HEAT PIPE EVACUATED TUBULAR COLLECTORS

In this example, two designs of heat pipe evacuated tubular collectors are investigated theoretically. The absorber fins in the evacuated tubes are either flat or curved and the fins have selective coating on both sides. This means that solar radiation from all directions can be utilized. An illustration of the evacuated tubes is given in Fig. 5. The tubes are connected to a heat exchanger manifold pipe where condensers for all tubes are placed.

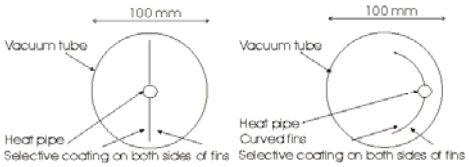

Fig. 5: The investigated evacuated tubular heat pipes.

Two new TrnSys [1] models for collectors with evacuated tubes with flat and curved fins are developed. The models take solar radiation from all directions into account. Further, due to the cylindrical tubes, depending on the position of the sun and the distance between the tubes, the tubes will be able to cast shadow on each other as illustrated in Fig. 6 and the solar irradiance can vary along the fin. For the curved fin model, the irradiance always varies along the fin as the incidence angle varies along the fin. Due to the variation in the solar irradiances along the fins, the traditional fin efficiency cannot be applied. Therefore, the heat transfer processes in the fin are solved in detail.

With the models, a parameter sensitivity analysis is carried out for the ground mounted evacuated tubular collectors installed in a solar heating plant. This analysis illuminates how the:

- different fin geometries
- collector tilt
- operating temperature
- tube distances
- distances between collector rows

influence the yearly thermal performance of the collector field.

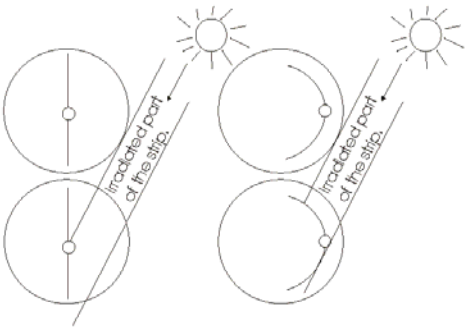

Fig. 6: The irradiated part of the fin for a given position of the sun.

2.1 Theory and definitions

In this section, the theory of the two collector models, for flat and curved fins respectively, will be summarized. The models are developed for the TrnSys simulation program. The models include both the evacuated tubular collectors and the heat exchanger manifold pipe, as illustrated in Fig. 7.

The power, P_u, from this system can be written as:

$$P_u = \dot{m} \cdot c_p \cdot (T_{manifold,outlet} - T_{manifold,inlet}) \quad (1)$$

$$P_u = P_{ETC} - P_{loss} - \frac{dQ_{manifold}}{dt} \quad (2)$$

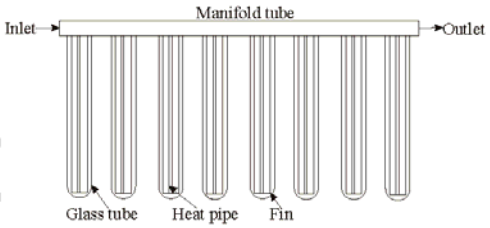

Fig. 7: The collector models include both the evacuated tubular collectors and the heat exchanger manifold pipe.

The power from the heat pipes, P_{ETC}, the heat loss from the manifold tube, P_{loss}, and the energy change in the manifold tube, $dQ_{manifold}$, can be written as:

$$P_{ETC} = UA_{manifold} \cdot (T_{heatpipe} - T_{manifold}) \quad (3)$$

$$P_{loss} = U_{loss} \cdot (T_{manifold} - T_{amb}) \quad (4)$$

with

$$T_{manifold} = \frac{T_{manifold,inlet} + T_{manifold,outlet}}{2} \quad (5)$$

The power from the heat pipes, P_{ETC}, is larger than zero if the temperature of the heat pipe working fluid, $T_{heatpipe}$, is larger than the lowest evaporation temperature and larger than the mean temperature in the manifold pipe, $T_{manifold}$. In other cases, P_{ETC} is zero. In order to determine the temperature of the heat pipe working fluid, the fin is discretized into a number of elements as illustrated in Fig. 8. The energy balances for the elements of the fin are:

i=1:

$$-\frac{\lambda \cdot \delta}{dx} \cdot L \cdot (T_i - T_{i+1}) + S_i \cdot L \cdot dx - U_L \cdot (T_i - T_{amb}) \cdot L \cdot dx = \frac{m_{fin} \cdot c_{p,fin}}{dt} \cdot (T_i^{new} - T_i^{old}) \quad (6)$$

1<i<n:

$$\frac{\lambda \cdot \delta}{dx} \cdot L \cdot (T_i - T_{i-1}) - \frac{\lambda \cdot \delta}{dx} \cdot L \cdot (T_i - T_{i+1}) + S_i \cdot L \cdot dx - U_L \cdot (T_i - T_{amb}) \cdot L \cdot dx = \frac{m_{fin} \cdot c_{p,fin}}{dt} \cdot (T_i^{new} - T_i^{old}) \quad (7)$$

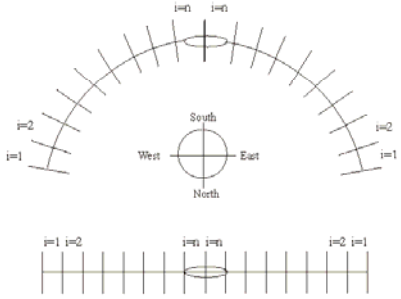

Fig. 8: The fins are discretized into a number of elements.

i=n:

$$\frac{\lambda \cdot \delta}{dx} \cdot L \cdot (T_i - T_{i-1}) - UA_{manifold} \cdot (T_i - T_{manifold}) + S_i \cdot L \cdot dx - U_L \cdot (T_i - T_{amb}) \cdot L \cdot dx = \frac{m_{fluid^*} \cdot c_{p,fluid^*}}{dt} \cdot (T_i^{new} - T_i^{old}) \quad (8)$$

Here, the solar radiation absorbed on the fin, S_i, is dependent on the position on the fin, due to varying incident angles (for curved fins) and due to possible shadows on the fin (for both flat and curved fins). The principles of determining the size and position on the fin of the shadows are described in [2].

The heat exchange capacity rate, $UA_{manifold}$, has a constant value larger than zero if T_n is larger than the lowest evaporation temperature and if T_n is larger than the mean temperature in the manifold pipe. In other cases, $UA_{manifold}$ is zero.

2.1.1 Solar radiation and view factors

The total solar radiation absorbed on the fin, S_i, can be written as:

$$S_i = S_{i,dir,front} + S_{i,dir,back} + S_{i,dif,sky,front} + S_{i,dif,sky,back} + S_{i,dir,ground,front} + S_{i,dir,ground,back} + S_{i,dif,ground,front} + S_{i,dif,ground,back} \quad (9)$$

where,

$$S_{i,dir,front} = (\tau\alpha)_e \cdot G_b \cdot K_\theta \cdot R_{b,front} \cdot R_{sun}$$
$$S_{i,dir,back} = (\tau\alpha)_e \cdot G_b \cdot K_\theta \cdot R_{b,back} \cdot R_{sun} \quad (10)$$

$$S_{i,dif,sky,front} = (\tau\alpha)_e \cdot G_d \cdot K_{\theta,dif} \cdot F_{col,sky,front}$$
$$S_{i,dif,sky,back} = (\tau\alpha)_e \cdot G_d \cdot K_{\theta,dif} \cdot F_{col,sky,back} \quad (11)$$

$$S_{i,dir,ground,front} = (\tau\alpha)_e \cdot G_b \cdot K_{\theta,gr} \cdot F_{col,dir,ground,front} \cdot \rho$$
$$S_{i,dir,ground,back} = (\tau\alpha)_e \cdot G_b \cdot K_{\theta,gr} \cdot F_{col,dir,ground,back} \cdot \rho \quad (12)$$

$$S_{i,dif,ground,front} = (\tau\alpha)_e \cdot G_d \cdot F_{ground,sky} \cdot K_{\theta,gr} \cdot F_{col,dif,ground,front} \cdot \rho$$
$$S_{i,dif,ground,back} = (\tau\alpha)_e \cdot G_d \cdot F_{ground,sky} \cdot K_{\theta,gr} \cdot F_{col,dif,ground,back} \cdot \rho \quad (13)$$

The incident angle modifier K_θ is calculated by:

$$K_\theta = 1 - \tan^a\left(\frac{\theta}{2}\right) \quad (14)$$

Here, the incident angle, θ, is defined as the incident angle on the absorber. The incident angle modifiers for diffuse radiation, $K_{\theta,dif}$, and ground reflected radiation, $K_{\theta,gr}$, are evaluated by equation (14) using $\theta=\pi/3$ [3].

An illustration of the view factors is given in Fig. 9 and a more detailed description of the view factors including reduction of the view factors to ground and sky due to the collector rows, is given in [4].

2.1.2 Numerical issues

In order to evaluate the performance of the evacuated tubular collectors on an annual basis, the above theory is implemented into three TrnSys types; two TrnSys types for the two collector designs and an additional TrnSys type for the view factor calculations. Concerning the two collector types, for each simulation time step the equations (1)-(8) are solved through an iteration loop. The iteration is stopped when the fin temperature difference from iteration to iteration is less than 0.00001 K and when the difference from iteration to iteration in power from the manifold is less than 0.01 W.

If the criteria are not reached the iteration loop stops after 100,000 iterations, and a warning is written to an output file. This seldom happens and the influence on the final result is insignificant. The fins are discretized into nine elements (18 elements in total), and a typical annual simulation of a collector array takes approximately 3 min. on a 2.8 GHz PC when a timestep of 0.05 h is used.

2.2 Parameter variations

In this section, it is illustrated how the model can be used for geometrical parameter studies. In the following examples it is assumed that the ground mounted evacuated tubular collector panels are operating in a solar heating plant at a constant operating temperature of 50°C in the heat exchanger manifold pipe throughout the year. The model data of the collector panel is given in Table 1. The collector performance is investigated for Uummannaq, Greenland, as summarized in Table 2. The albedo is set higher during a large part of the year due to snow on the ground.

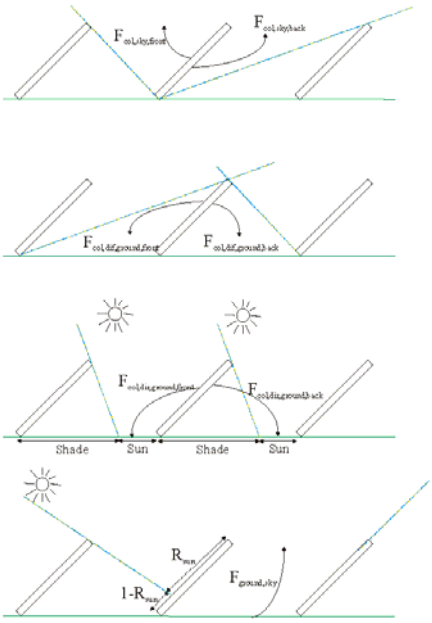

Fig. 9: An illustration, based on three collector rows, of the view factors used in the model. R_{sun} includes the effect of one row shadowing the next row.

Table 1: Data describing the collector in the model.

Tube length, L	[m]	2
Glass tube radius, r_c	[m]	0.05
Absorber radius for curved fin, r_p	[m]	0.04375
Fin width for curved fin, w_c (corresponding to a curved fin angle of 164°)	[m]	0.125
Fin width (for flat fin), w_f	[m]	0.0875
Fin thickness	[m]	0.0002
Fin conductivity, k_{fin}	[W/mK]	216
Tube centre distance, C	[m]	0.125
Tube heat loss coefficient, k_{tube} based on absorber front side area	[W/m²K]	2.43
Effective transmittance absorbtance product, $(\tau\alpha)_e$	[-]	0.84
Incident angle modifier constant, a	[-]	3.8
Manifold heat loss coefficient, $k_{manifold}$	[W/K/m]	0.134
Manifold heat exchange rate per connection, $UA_{manifold}$	[W/K]	10
Operating temperature in manifold	[°C]	50
Collector heat capacity, $C_{collector}$	[kJ/K/tube]	1.9
Distance between collector rows	[m]	10

Table 2: Summarized data for Uummannaq, Greenland.

Location	Unit	Uummannaq, GL [5]
Latitue.	[°]	71
Longitude	[°]	52
$T_{a,average}$	[°C]	-4.2
G_{global}	[kWh/m²]	888
$G_{diffuse}$	[kWh/m²]	409
Albedo	[-]	0.2 (15/6-14/9) or 0.7 (15/9-14/6)

2.2.1 View factors

To get an understanding of the geometry included in the models, illustrations of some of the view factors for different conditions is given below. The view factors are calculated for a collector tilt of 60° and for infinite distance between the collector rows. For different tube centre distances Fig. 10 and Fig. 11 shows the view factor from one tube to the two neighbour tubes, $F_{tube,tube}$, and the view factors to the sky and ground from the collector's front and back side respectively.

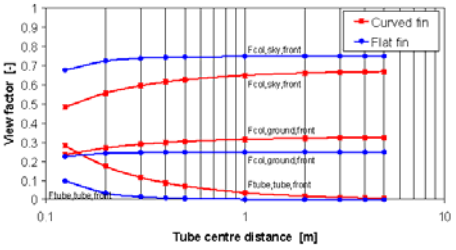

Fig. 10: View factors for the collector front side.

For the collector front side, it can be seen that the flat fin collector has a larger view factor to the sky, a smaller view factor to the ground and a smaller view factor between the tubes compared to the curved fin collector. This is because parts of the curved fin – due to the curve – face the neighbour tubes and the ground more than the flat fin. Further, as expected, the view factors between the tubes decreases with increasing tube centre distances.

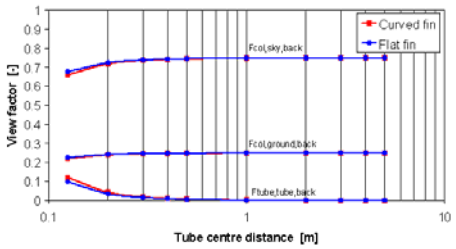

Fig. 11: View factors for the collector back side.

For the collector back side, it can be seen that there is almost no difference between the curved and the flat fin. Here the reason is that, when calculating the view factors, the back side of the curved fin can be treated as a flat fin placed in the opening of the curved fin.

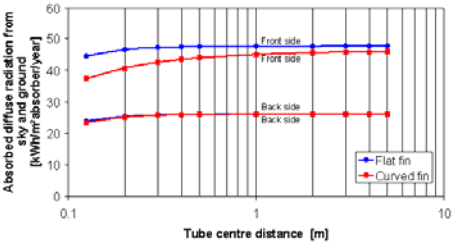

Fig. 12: Absorbed diffuse sky and ground reflected radiation.

Fig. 12 shows the yearly diffuse sky and ground reflected radiation absorbed by the fin per m² front side absorber.
For the collector back side, it can be seen that, just as for the view factors, there is almost no differences between the curved and the flat fin. For the collector front side it is clear that the flat fin absorbs more diffuse radiation than the curved fin.

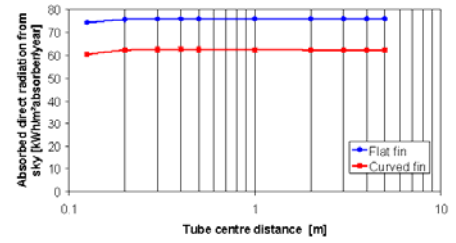

Fig. 13: Absorbed direct radiation.

Finally, Fig. 13 shows the direct radiation absorbed by the front side of the fins. As expected, due to the view factors between fins and sky, the flat fin absorbs more direct radiation per m² front side absorber on a yearly basis. As it looks like the flat fin collector is more efficient, it must be pointed out that the absorbed energy quantities are given per m²

absorber area and that the curved fin absorber area is 45% larger than the flat fin absorber area.

2.2.2 Temperature profiles on the fin

Before going into thermal performance analyses, some examples of the temperature distribution on the fins are given. For a summer day (31/7), Fig. 14 and Fig. 15 show the temperature profile at solar time 9 AM, 12 PM and 3 PM for the curved and the flat fin respectively. At these three times there are no shadows from the neighbour tubes. The temperature distribution on the curved fin is symmetrical around the heat pipe at 12 PM whereas the east side of the fin is warmer during the morning and the west side of the fin is warmer during the afternoon.

This clearly illustrates the influence of the distribution of the solar radiation on the fin and it explains why the traditional fin efficiency, F, cannot be applied when analysing this type of collector in detail. As expected for the flat fin, there is symmetry in the temperature distribution at all three times. The differences in the temperature level for the three times are due to the weather conditions.

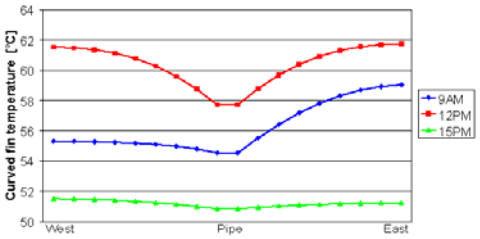

Fig. 14: The temperature distribution on the curved fin in the morning, at noon and in the afternoon of a summer day.

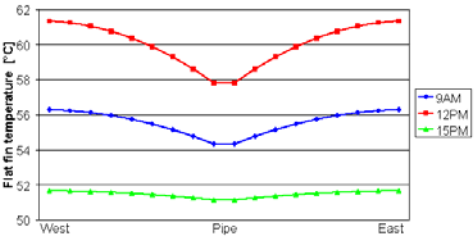

Fig. 15: The temperature distribution on the flat fin in the morning, at noon and in the afternoon of a summer day.

2.2.3 Collector tilt

Fig. 16 shows the thermal performance per tube as a function of the collector tilt. The figure shows that the optimum tilt is about 45° for the flat fin collector and slightly higher for the curved fin collector. The reason is most likely related to the differences in the view factors for the two collectors. As the curved fin collector, due to the design, sees more of the ground compared to the flat fin collector, the curved fin collector can utilize the ground reflected radiation better than the flat fin collector and consequently the optimum tilt is larger for the curved fin collector than for the flat fin collector. The curved fin collector performs better than the flat fin collector as the curved fin absorber area is larger than the flat fin absorber area.

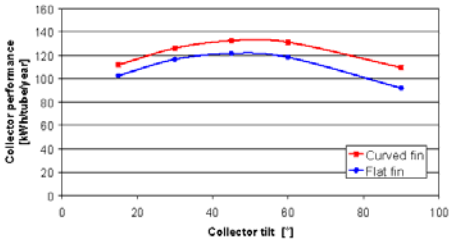

Fig. 16: The thermal performance per tube as a function of the collector tilt.

2.2.4 Operating temperature

Fig. 17 shows the thermal performance as a function of the operating temperature in the manifold tube.

As expected the thermal performance decreases with increasing temperature level due to the increasing heat loss. Further, it can be seen that the curves are about to cross at a temperature of 90°C. The reason is that the heat loss is larger for the curved fin collector compared to the flat fin collector as the heat loss coefficient (the same for the two collectors) is based on the absorber front side area and the curved absorber is larger than the flat fin absorber.

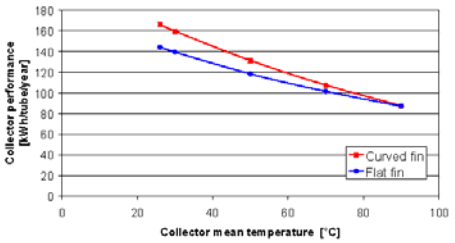

Fig. 17: The thermal performance per tube as a function of the operating temperature in the manifold tube.

2.2.5 Tube centre distances

Fig. 18 shows the thermal performance per tube as a function of the tube centre distance. The thermal performance increases for increasing tube centre distances up to about 0.3 m, due to reduced shaded areas, reduced view factors between the tubes and thus increased view factors to sky and ground. For even larger distances the utilized energy decreases again, due to the increasing heat loss from the manifold pipes.

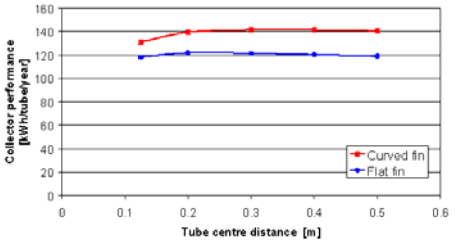

Fig. 18: The thermal performance per tube as a function of the tube centre distance.

2.2.6 Collector rows distances

Finally, Fig. 19 shows the thermal performance per tube as a function of the distance between the collector rows. It can be seen that thermal performance increases rapidly when the row distance increases from 1 m to 10 m. Further increase in the row distance has less impact on the thermal performance. The reason for the increase in thermal performance is that with increasing distances the shadows from neighbour rows on the collector (see Fig. 9 bottom) decreases and the view factor from the collector to ground and sky increases. It must be noticed that the heat loss in the pipes connecting the collector rows is not included in this analysis.

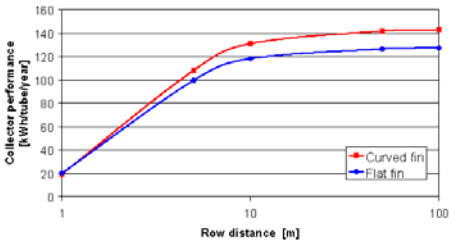

Fig. 19: The thermal performance per tube as a function of the distance between the collector rows.

2.3 Summary

Two designs of ground mounted heat pipe evacuated tubular collectors operating in a solar heating plant are investigated theoretically. The absorber fins inside the evacuated tubes are either flat or curved and the surfaces of the fins have selective coating on both sides. Two new TrnSys models for evacuated tubular collectors are developed. The models calculate in detail the heat transfer processes of the absorber fins.

It is illustrated how the model can be used for geometrical parameter studies. For example, it is investigated how fin geometry, collector tilt, operating temperature, tube distances and distances between collector rows influences the yearly thermal collector performance.

3 RESEARCH EXAMPLE 2: ALL-GLASS EVACUATED TUBULAR COLLECTORS

All-glass evacuated tubular collectors are based on double glass tubes where the outside of the inner glass wall is treated with an absorbing selective coating and the evacuated space is between the tubes as illustrated in Fig. 20.

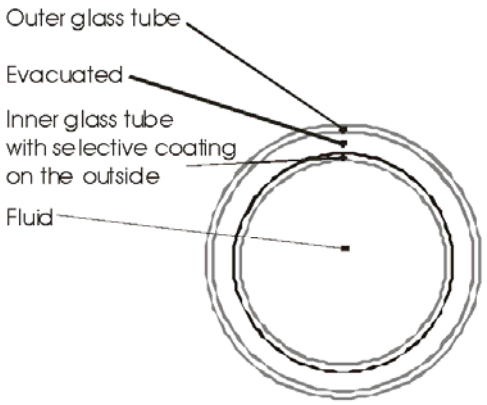

Fig. 20: Design of an All-glass evacuated tube.

A collector design based on horizontal tubes connected to a manifold pipe is especially popular due to its low cost. An illustration of the collector design is shown in Fig. 21.

The collector fluid enters the bottom of the square manifold channel and leaves at the top of the manifold channel. The intended flow inside the glass tubes is indicated with the arrows. The flow is primarily naturally driven, as the walls of the tubes are hot due to the solar radiation. However it is unclear, how the operating conditions and the collector geometry influence the flow structures in the tubes and thus the collector performance.

The objective of this work is to investigate the heat transfer and the flow structures inside the tubes for different flow rates and collector geometries by means of Computational Fluid Dynamics (CFD).

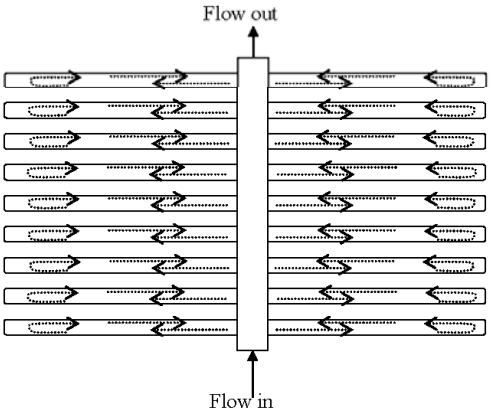

Fig. 21: Illustration of an All-glass evacuated tubular collector with horizontal tubes.

3.1 Numerical investigations

To solve the flow and energy equations in the glass tubes, a simulation model of the flow in the tubes is developed using the CFD code Fluent 6.1 [6]. As illustrated in Fig. 22, only one section of the collector with two horizontal tubes placed in a vertical plane is investigated.

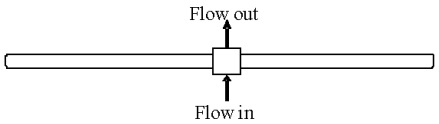

Fig. 22: One section of the collector with two horizontal tubes is investigated.

Steady state numerical solutions are obtained for laminar flow with the Boussinesq approximation for buoyancy modelling. The velocity-pressure coupling is treated by using the SIMPLE algorithm and the First Order Upwind scheme is used for the momentum and energy terms.

3.1.1 Geometry

The model consists of the inner boundaries of the geometry. The outer glass tube, the evacuated space between the two glass tubes and the wall thickness of the inner glass tube are

not included in the model. Also the outer casing and the insulation material of the manifold channel are not included in the model. This means that no solids are simulated – only the fluid is included in the model. The conduction in the inner glass wall is however included in the model. The geometry is summarized in Table 3.

TABLE 3: GEOMETRY OF THE NUMERICAL MODELS.

Side length of manifold channel:	0.06 m
Glass tube inner diameter:	0.037 m
Glass tube outer diameter (used in manifold channel):	0.047 m
Length of glass tube exposed to solar radiation:	0.59 m 1.17 m 1.47 m
Number of computational cells:	428682 738708 948499
Illustration of geometry:	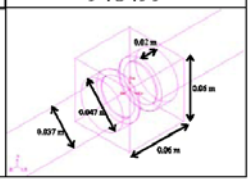

The computational mesh is constructed in the pre-processing program Gambit 2.0.4 [7]. The number of computational cells depends on the length of the tubes and is given in Table 3.
Fig. 23 shows a close up of the mesh near the manifold channel.

3.1.2 Boundary conditions

The solar irradiance is simulated as a distributed heat flux on the tube wall. The flux varies from 0 W/m² to 1150 W/m² as shown in Fig. 24. The average flux on the tube wall is 566 W/m².

The heat loss from the tubes is modelled with a heat loss coefficient of 0.85 W/m²K [8] and a constant ambient temperature of 293 K. The heat loss coefficient is related to the absorber area. The manifold channel is assumed to have zero heat loss.

Five different inlet mass flow rates of respectively 0.05 kg/min, 0.4 kg/min, 1 kg/min, 3 kg/min and 10 kg/min have been computed.

The inlet velocity profile has been found by first making a computation with a uniform inlet velocity profile. The outlet velocity profile from this simulation has then been used as the inlet velocity profile for the final simulation.
The inlet temperature has been 333 K during all computations. A 40% propylene-glycol/water mixture has been used as working fluid.

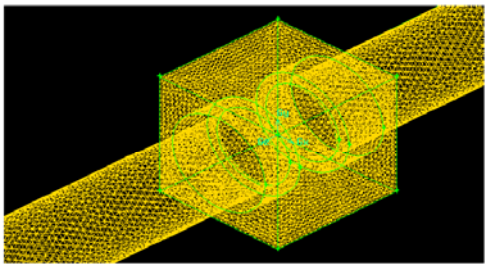

Fig. 23: The mesh near the square manifold channel.

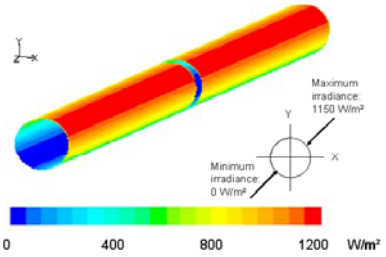

Fig. 24: Distribution of the heat flux on the inner glass tubes.

3.2 Results

The presented results will include illustrations of flow patterns in the vertical centre plane of the model near the manifold channel and in the manifold outlet plane. Further, some overall analyses of the "collector" performance as a function of tube lengths and mass flow rates will be presented.

3.2.1 Flow distribution

For a tube length of 1.17 m, the left column in Fig. 25 shows velocity vectors in the vertical tube centre plane near the manifold channel for the five investigated inlet mass flow rates.

At the smallest mass flow rate (top-left picture) it can be seen how the fluid flows directly from the inlet in the manifold channel out in the two horizontal tubes. The fluid returns to the manifold channel along the top of the tubes. The two flows from the two tubes exits at the outlet with a profile, which is clearly formed by the flows in the tubes.

The flow patterns for the next two flow rates look similar to the flow pattern for the lowest flow rate; however, there is one significant difference. Due to the larger inlet velocities, the flow rises higher in the manifold channel before it, due to buoyancy forces, turns down to the tube bottom wall and flows out in the tubes. The differences in the forced- and buoyancy driven flows are evident just by seeing how far up in the manifold tube the flow rises.

For the two highest flow rates it is clear that some of the flow passes directly through the manifold channel without entering the tubes. Therefore, the outlet velocity profiles look different for the highest flow rates compared to the outlet velocity profiles for the lowest flow rates.

The right column in Fig. 25 shows the velocity contours in the outlet plane. It can be seen how the velocity pattern changes from being dominated by the two flows from the tubes for the lowest inlet flow rates to, for the highest flow rates, being dominated mainly by the inlet flow.

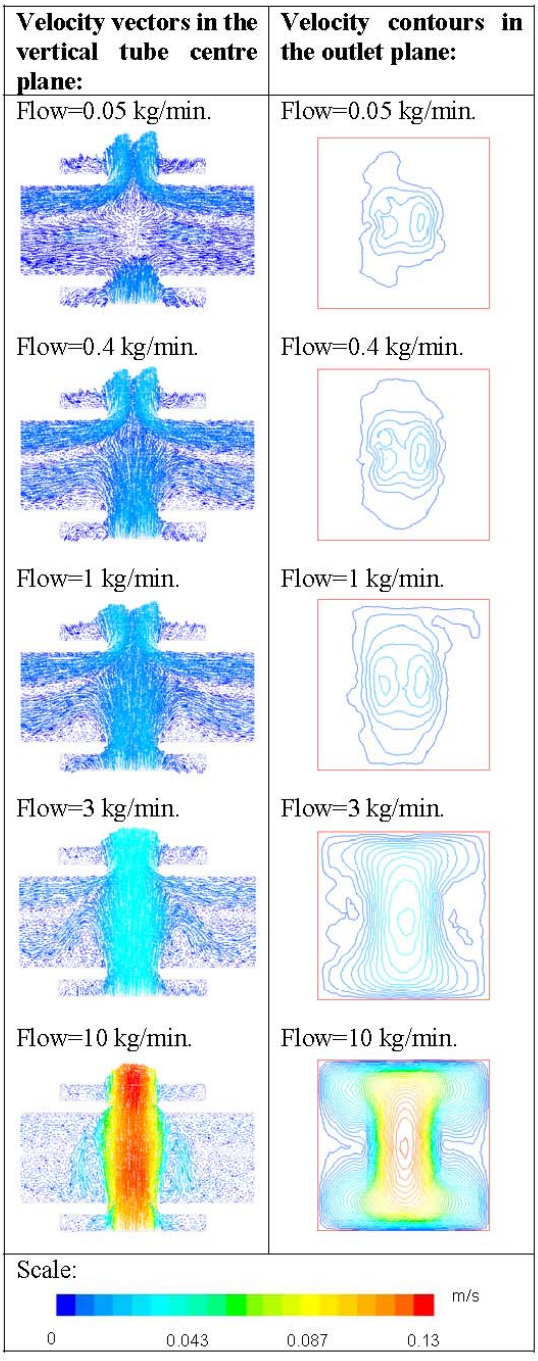

Fig. 25: Velocity patterns in the vertical tube centre plane (left column) and in the outlet plane (right column). Tube length: L=1.17 m.

3.2.2 Thermal performance

The thermal performance is investigated by calculating efficiencies for the different combinations of flow rates and tube lengths. The efficiency, η, is defined as the ratio between the power out of the collector, $P_{collector}$, and the distributed heat flux absorbed by the collector, P_{solar}:

$$\eta = \frac{P_{collector}}{P_{solar}}$$

Notice that this efficiency cannot be compared with the traditional way of defining the collector efficiency as optical losses are not included in the efficiency used here.

Fig. 26 shows the efficiency as a function of the mass flow rate. The efficiency is highest for flow rates around 0.4 kg/min – 1 kg/min. The explanation for this result can be found in Fig. 27, which shows the mean temperature in the collector as a function of the mass flow rate. For the largest inlet flow rates (3 kg/min – 10 kg/min) a large part of the fluid flows directly through the manifold channel leaving only a smaller part flowing out in the tubes. Therefore, the average temperature in the whole collector rises.
This leads to a higher heat loss and thus a lower efficiency. For the lowest flow rate (0.05 kg/min) almost all the inlet flow goes out in the tubes, but now the flow is so small that this alone leads to an increased average temperature in the whole collector.

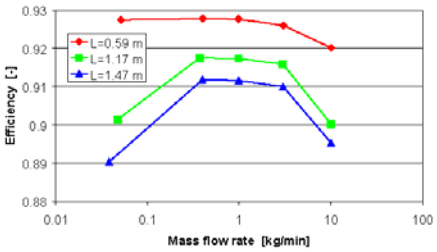

Fig. 26: The efficiency as a function of the mass flow rate.

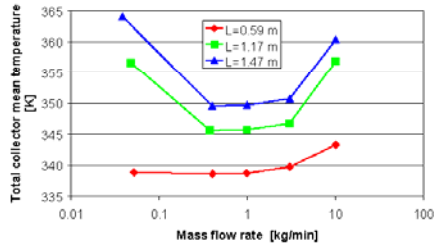

Fig. 27: The mean temperature in the total collector as a function of the mass flow rate.

That the efficiency in fact decreases with increasing average temperatures in the whole collector is very clear in Fig. 28 Here each dot represents an efficiency found at a given inlet flow rate.
All the dots together form an almost straight line with a tilt that shows how the efficiency decreases with increasing heat loss caused by increasing average temperatures in the whole collector. The collector with the shortest tube has the highest efficiency and vice versa.

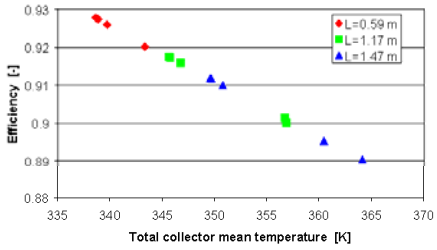

Fig. 28: The efficiency as a function of mean temperature in the whole collector.

Finally, Fig. 29 shows the efficiency as a function of the average of the inlet- and outlet temperature. As in Fig. 26 and in Fig. 28 it can be seen that the highest efficiency is achieved for the shortest tube length.

The results further show that the inlet mass flow rate has a relatively small influence (1-2 %) on the resulting efficiencies. This might seem strange considering the large differences in the flow patterns near the manifold channel (Fig. 25).

The main reason is that the flow in the tubes at a distance from the manifold channel is relatively unaffected by the inlet flow.

For a tube length of L=1.17 m, Fig. 30 shows the maximum velocity magnitude as a function of the distance from the manifold centre. For the varying inlet flows, the figure shows that close to the manifold channel there are differences in the maximum velocity magnitude but further out in the tubes there are almost no differences in the maximum velocity magnitude.
This explains why the absolute differences in the collector efficiencies are so small for the varying inlet flow conditions.
Fig. 30 also shows that the flows out in the tubes are:

- largest for an inlet flow of 0.4 kg/min
- 2nd largest for an inlet flow of 1 kg/min
- 3rd largest for an inlet flow of 3 kg/min
- 2nd smallest for an inlet flow of 0.05 kg/min and
- smallest for an inlet flow of 10 kg/min

This corresponds nicely with the results presented in Fig. 26 where the order of efficiencies is the same.

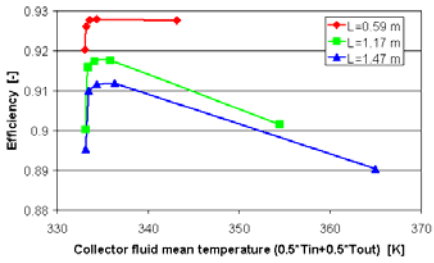

Fig. 29: The efficiency as a function of the average of the inlet- and outlet temperature.

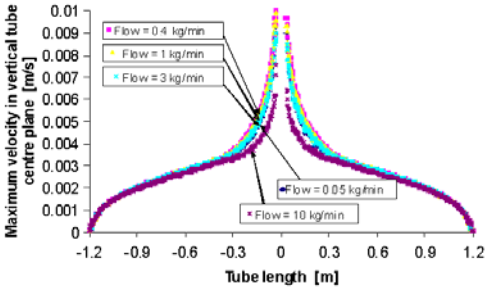

Fig. 30: Maximum velocity magnitude in the tubes (outside the manifold channel) in the vertical centre plane.

Finally, it should be mentioned that another reason for the small differences in the calculated efficiencies is that the heat loss coefficient for the tubes is very small. Due this low heat loss coefficient, the differences in the mean temperature in the whole collector have an only minor influence on the final efficiency.

3.3 Summary

Heat transfer and flow structures inside All-glass evacuated tubular collectors for different operating conditions are investigated by means of Computational Fluid Dynamics (CFD). The investigations are based on a collector design with horizontal tubes connected to a vertical manifold channel.
Three different tube lengths varying from 0.59 m to 1.47 m have been modelled with five different inlet mass flow rates varying from 0.05 kg/min to 10 kg/min with a constant inlet temperature of 333 K. Under these operating conditions the results showed that:

- the collector with the shortest tube length achieved the highest efficiency
- the optimal inlet flow rate was around 0.4-1 kg/min
- the flow structures in the glass tubes were relatively uninfluenced by the inlet flow rate

Generally, the results showed only small variations in the efficiencies. This indicates that the collector design is well working for most operating conditions.

4 CONCLUSION AND OUTLOOK

In this paper two research examples on evacuated tubular collectors are given. The first example concerns development of theoretical models for Heat pipe evacuated tubular collectors. In the second example heat transfer and flow structures inside All-glass evacuated tubular collectors for different operating conditions are investigated by means of Computational Fluid Dynamics (CFD).

For the heat pipe investigations, ground mounted Heat pipe evacuated tubular collectors operating in a solar heating plant are investigated theoretically. It is illustrated how the developed model can be used for geometrical parameter studies. For example, it is investigated how fin geometry, collector tilt, operating temperature, tube distances and distances between collector rows influences the yearly thermal collector performance.

The All-glass investigations were based on a collector design with horizontal tubes connected to a vertical manifold channel. With different glass tube lengths and for varying flow rates it was shown that the collector with the shortest tube length achieved the highest efficiency and the optimal inlet flow rate was around 0.4-1 kg/min. However, generally the All-glass results showed only small variations in the efficiencies. This indicates that the collector design is well working for most operating conditions.

Further work:

Parallel to the theoretical work, the investigated Heat pipe and All-glass evacuated tubular collectors will be tested side-by-side in an outdoor test facility. Among other things, the measured performances will be used to a final validation of the theoretical models and the thermal performance of differently designed evacuated tubular collectors will be compared. Based on the findings and on economy considerations, optimum designed evacuated tubular collectors for Arctic latitudes will be recommended.

5 ACKNOWLEDGEMENTS

This study is financed by the VILLUM KANN RASMUSSEN FOUNDATION.

6 REFERENCES

[1] Klein, S.A. et al., "TRNSYS 14.2", University of Wisconsin Solar Energy Laboratory, 1996.

[2] Shah, L.J., Furbo, S., "Modelling Shadows on Evacuated Tubular Collectors with Cylindrical Absorbers", Journal of Solar Energy Engineering, Transactions of the ASME, 2005 (In press).

[3] Gordon J. (ed.). Solar Energy. The State of the Art. ISES Position papers. James & James, London. ISBN: 1-902916-23-9, (2001).

[4] Shah, L.J., Furbo, S., "Utilization of Solar Radiation at High Latitudes with Evacuated Tubular Collectors" NorthSun 2005, Proceedings, In press.

[5] Kragh J. et al. "Grønlandske vejrdata. Nuuk. Uummannaq" Department of Civil Engineering, Technical University of Denmark, Nov. 2002.

[6] Fluent 6.1 User's Guide (2003). Fluent Inc. Centerra Resource Park 10 Cavendish Court Lebanon, NH 03766

[7] Gambit 2 User's Guide (2001). Fluent Inc. Centerra Resource Park 10 Cavendish Court Lebanon, NH 03766

[8] Qin l. and Furbo S. (1999) *Vakuumrørsolfangere fra Kina*. Report R-032. Department of Buildings and Energy, Technical University of Denmark.

7 NOMENCLATURE

a	Incident angle modifier constant, -
C	Tube centre distance, m
$C_{collector}$	Collector heat capacity, kJ/K/tube
$c_{p,fin}$	Heat capacity of fin material, J/kgK
$c_{p,fluid*}$	Average heat capacity of fin material and working fluid in heat pipe, J/kgK
$dQ_{manifold}$	Energy change in the manifold pipe, J
dt	Timestep, s
dx	Width of discretization element, m
$F_{col,dif,ground,back}$	View factor from the collector back side to the part of the ground with diffuse solar radiation, -
$F_{col,dif,ground,front}$	View factor from the collector front side to the part of the ground with diffuse solar radiation, -
$F_{col,dir,ground,back}$	View factor from the collector back side to the part of the ground with direct solar radiation,-
$F_{col,dir,ground,front}$	View factor from the collector front side to the part of the ground with direct solar radiation,-
$F_{col,sky,back}$	View factor from the collector back side to the sky, -
$F_{col,sky,front}$	View factor from the collector front side to the sky, -
$F_{ground,sky}$	View factor the ground to the sky, -
$F_{tube,tube}$	View factor from one tube to the neighbour tubes, -
G_b	Beam radiation on horizontal, W/m²
G_d	Diffuse radiation on horizontal, W/m²
$G_{diffuse}$	Yearly diffuse radiation on horizontal, kWh/m²
G_{global}	Yearly global radiation, kWh/m²
K_θ	Incident angle modifier for direct radiation, -
$K_{\theta,dif}$	Incident angle modifier for diffuse radiation, -
$K_{\theta,gr}$	Incident angle modifier for ground reflected radiation, -
L	Tube length, m
m_{fin}	Mass of discretized fin element, kg
m_{fluid*}	Average mass of fin material and working fluid in heat pipe, kg
P_{ETC}	Power from heat pipes, W
P_{loss}	Heat loss from manifold pipe, W
P_u	Power from collector, W
$P_{collector}$	Power from collector, W
P_{solar}	Solar radiation absorbed by absorber, W
$R_{b,back}$	Geometric factor, -
$R_{b,front}$	Geometric factor, -
r_c	Glass tube radius, m
r_p	Absorber radius for curved fin, m
R_{sun}	Part of tube irradiated by direct radiation due to row shadows, -
S_i	Solar radiation absorbed on element i, W/m²
$S_{i,dif,sky,front}$	Diffuse sky radiation absorbed on the absorber front side, W/m²
$S_{i,dif,ground,back}$	Ground reflected diffuse radiation absorbed on the absorber back side, W/m²
$S_{i,dif,ground,front}$	Ground reflected diffuse radiation absorbed on the absorber front side, W/m²
$S_{i,dif,sky,back}$	Diffuse sky radiation absorbed on the absorber back side, W/m²
$S_{i,dir,back}$	Direct radiation absorbed on the absorber back side, W/m²
$S_{i,dir,front}$	Direct radiation absorbed on the absorber front side, W/m²
$S_{i,dir,ground,front}$	Ground reflected direct radiation absorbed on the absorber front side, W/m²
$S_{i,dir,ground,back}$	Ground reflected direct radiation absorbed on the absorber front side, W/m²
$T_{a,average}$	Yearly average ambient temperature, °C
T_{amb}	Ambient temperature, °C
T_{amb}	Ambient temperature, °C
$T_{heatpipe}$	Temperature of the heat pipe working fluid, °C
T_i	Temperature of element i, °C
T_{i+1}	Temperature of element i+1, °C
T_{i-1}	Temperature of element i-1, °C
T_i^{new}	New temperature of element i, °C
T_i^{old}	Old temperature of element i, °C
$T_{manifold}$	Mean temperature in manifold, °C
$T_{manifold,inlet}$	Inlet temperature to manifold, °C
$T_{manifold,outlet}$	Outlet temp. from manifold, °C
$UA_{manifold}$	Manifold heat exchange rate, W/K
U_L	Tube heat loss coefficient, W/m²K
U_{loss}	Manifold heat loss coef., W/K/m
w_c	Fin width for curved fin, m
w_f	Fin width for flat fin, m
δ	Fin thickness, m
λ	Fin thermal conductivity, W/mK
ρ	Ground albedo, -
$(\tau\alpha)e$	Transmittance absorbance prod., -

Bilag 3: Artikel optaget i Installationsnyt - Specialhæfte nr. 46/2005. TechMedia A/S.

Energi i kulden

Vakuumrørsolfangere til Arktis

Af Louise Jivan Shah, Associated Research Professor, PH.D., DTU

I 2003 bevilgede Villum Kann Rasmussen Fonden midler til et treårigt forskningsprojekt vedrørende vakuumrørsolfangere.
Projektet er en del af en større satsning fra Fonden vedrørende »Bæredygtigt arktisk byggeri i det 21. århundrede«. Projektet er ca. halvvejs i forløbet og denne artikel berører nogle af de foreløbige forskningsresultater.

Solstråling ved nordlige breddegrader

Solenergi er den reneste og naturligste energiform, vi overhovedet har. Solindfaldet er så stort på kloden – og i arktiske egne – at der er mulighed for at udnytte solenergi i stort omfang.
Det årlige antal timer med mulighed for solskin er stort set det samme, uanset hvor på kloden vi befinder os. *Figur 1* og *figur 2* viser til gengæld, at fordelingen af solstrålningen over årets måneder afhænger stærkt af breddegraden: Jo højere mod nord vi befinder os, des større del af solindfaldet finder sted i sommermånederne.
Solens bane over himlen er også stærkt afhængig af breddegraden. Jo højere mod nord vi befinder os, des lavere står solen på himlen, og des større er dagsvariationen af retningen til solen.
Nord for polarcirklen er solen således om sommeren på himlen 24 timer i døgnet, og retningen til solen gennemløber i løbet af 24 timer alle kompassets retninger.

Vakuumrørsolfangere

Når et solfangerdesign skal udvikles til arktiske breddegrader, må det således være en fordel, at designet bedst muligt udnytter solens bane.
På grund af meget lave lufttemperaturer er det også en fordel, hvis solfangeren har en lav varmetabskoefficient, således at mindst muligt af den absorberede solenergi tabes til omgivelserne.
Endelig må solfangeren være velegnet til at opfange reflekteret solstråling, hvilket der på grund af sne er meget af på de arktiske breddegrader.
Vakuumrørsolfangere kan designes, så de opfylder disse krav og de kan udformes på forskellige måder.

Heat Pipe vakuumrørsolfangere

Heat Pipe vakuumrørsolfangere består af en række cylinderformede glasrør, som øverst er koblet til en kondensator/varmeveksler-enhed.
Inde i glasrørene med vakuum er placeret absorbere med selektiv belægning og et rør, som indeholder et varmetransporterende medium, f.eks. vand.
Det varmetransporterende medium fordamper ved et lavt temperaturniveau, når absorberen opvarmes af solens stråler.
Dampen stiger opad i røret til en kondensator, hvor dampen kondenserer og derved afgiver varme til solfangervæsken, som pumpes gennem kondensator/varmeveksler-enheden.
I kondensatoren kondenserer det varmetransporterende medium,

Figur 1.

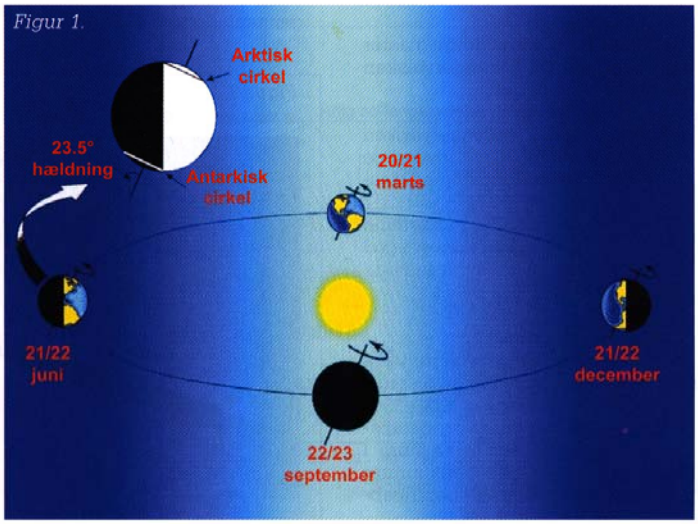

der som væske flyder ned til bunden af røret, hvor det igen fordamper, hvis temperaturen er høj nok, hvorefter processen gentages.
Figur 3 illustrerer Heat Pipe princippet.

All-glass vakuumrørsolfangere

All-glass vakuumrørsolfangere er udført på en anden og lidt mere simpel måde end heat pipe vakuumrørsolfangerne.
De er baseret på dobbeltglasrør *(se figur 4)* med vakuum i mellemrummet mellem glassene.
De udvendige overflader af de inderste glasrør har en høj absorptans og en lav emittans, og virker som solfangerens absorber.

Klima	Bredde-grad	Længde-grad	Gennemsnitlig udeluft-temperatur	Global solstråling	Diffus solstråling på vandret	Omgivelsernes reflektions-koefficient
	[°]	[°]	[°C]	[kWh/m²]	[kWh/m²]	[-]
København [5]	56	12	7.8	1002	510	0.2
Uummannaq Grønland [6]	71	52	-4.2	888	409	0.2 (15/6 - 14/9) 0.7 (15/9 - 14/6)

Tabel 1. Vejrdata (årsværdier) for København og Uummannaq.

Figur 2.

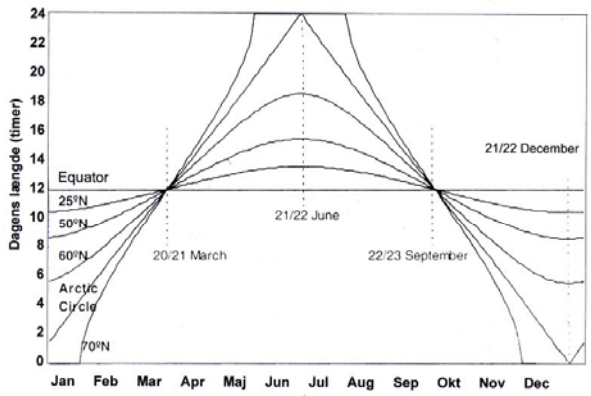

Når solen skinner på glasrøret, bliver det indvendige glasrør derfor meget varmt.
Varmen fra det indvendige glasrør kan overføres til solfangervæsken på forskellige måder:

- Enten kan solfangervæsken strømme inden i det indvendige glasrør i direkte kontakt med glasvæggen.
- Solfangervæsken kan strømme igennem et metalrør, som er i god termisk kontakt med det indvendige glas.

Velegnet til Arktis

Vakuumrørsolfangere synes at være velegnede til arktiske forhold, fordi:

- Solfangeren har en lav varmetabskoefficient. Da der er vakuum i begge typer af vakuumrør solfangerne er varmetabet fra absorberne på grund af konvektion og varmeledning meget lille. Varmetabskoefficienten for vakuumrørsolfangere er derfor meget mindre end varmetabskoefficienten for almindelige plane solfangere.
- Solfangerdesignet kan udnytte solens bane om sommeren, hvor solen kommer fra alle retninger gennem døgnet. All-glass vakuumrørsolfangerne har cylinderformet absorbere, og i Heat-pipe vakuumrørsolfangerne kan absorberfinnen bøjes, så den følger glasrørets krumning.
- Den krumme/cylinderformede absorberform gør også, at solfangeren bedre kan udnytte reflekteret stråling fra omgivelserne.

Teoretiske modeller

I forskningsprojektets første år har arbejdet været koncentreret om udvikling af teoretiske modeller til beregning af termiske ydelser for vakuumrørsolfangere, der udnytter solstrålingen fra alle retninger.
Traditionelle solfangerteorier fra litteraturen er udviklet med henblik på almindelige plane solfangere med plane absorbere.
Disse teorier har ikke direkte kunnet anvendes i forbindelse med vakuumrørsolfangerne, da absorberne er cylinderformede.
Derfor er der udviklet to nye teoretiske solfangermodeller til vakuumrørsolfangere med cylinderformede absorbere.
Modellerne er udviklet til hhv. All-glass og Heat-pipe vakuumrørsolfangerne. Baggrundsteorien kan studeres i [1, 2, 3].
Nedenfor er givet et eksempel på

Figur 3.

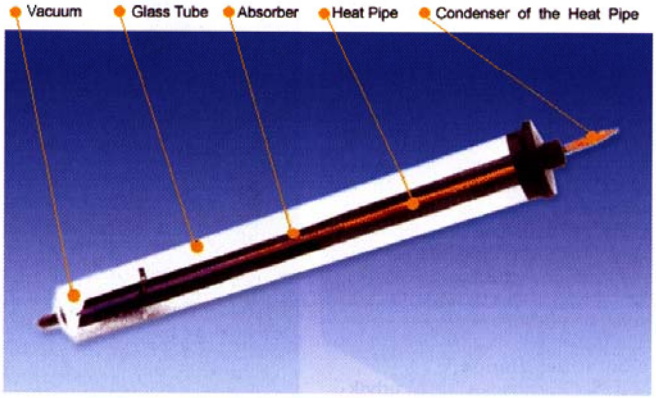

anvendelsen af All-glass solfangermodellen.

Modellering af All-glass vakuumrørsolfangere

Modellen tager udgangspunkt i den traditionelle plane solfangerteori, som integreres over den cylinderformede absorber.

Modellen kan præcist bestemme skyggeeffekterne fra rør til rør *(se figur 5)*, ligesom den kan regne på, hvordan solfangeren udnytter solstrålingen fra alle kompassets retninger.

Beregninger med den teoretiske solfangermodel er sammenholdt med målinger på en prototype solfanger og det viser sig, at modellen

Figur 4.

gengiver »virkeligheden« med stor nøjagtighed.

Modellen er herefter videreudviklet, så den nu kan indgå i simuleringsprogrammet TRNSYS [4]. Dette

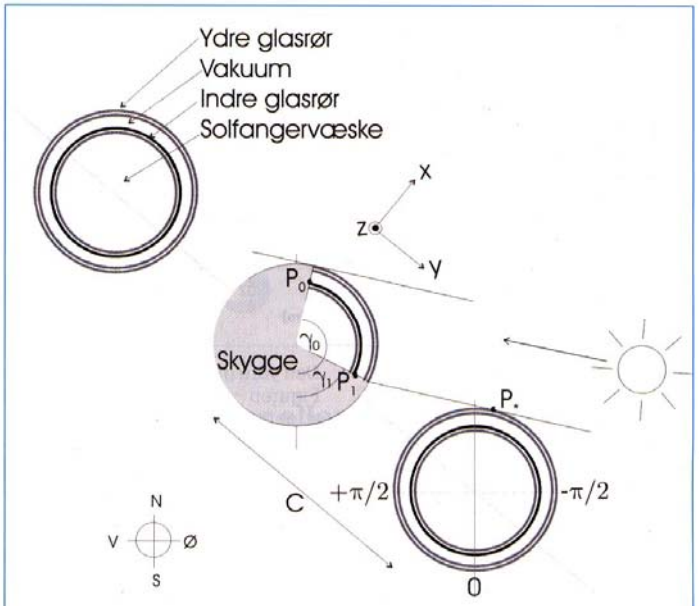

Figur 5.

amerikanske simuleringsprogram er et komponentbaseret program, som er det mest anvendte og anerkendte simuleringsprogram til solvarmeanlæg.

Geometriske parametre

Nedenfor illustreres det, hvordan All-glass modellen kan benyttes til f.eks. geometriske parameterundersøgelser.

Vakuumrørsolfangeren antages at være installeret i en solvarmecentral, hvor den opererer ved en konstant middeltemperatur på 50°C.

Solfangerydelsen er undersøgt for to klimaer, hhv. for København og Uummannaq (Grønland).

Årlige gennemsnitsdata for klimaerne er vist i *tabel 1*.

Omgivelsernes reflektionskoefficient er for en stor del af året højere i Uummannaq end i København på grund af sneen.

Figur 6.

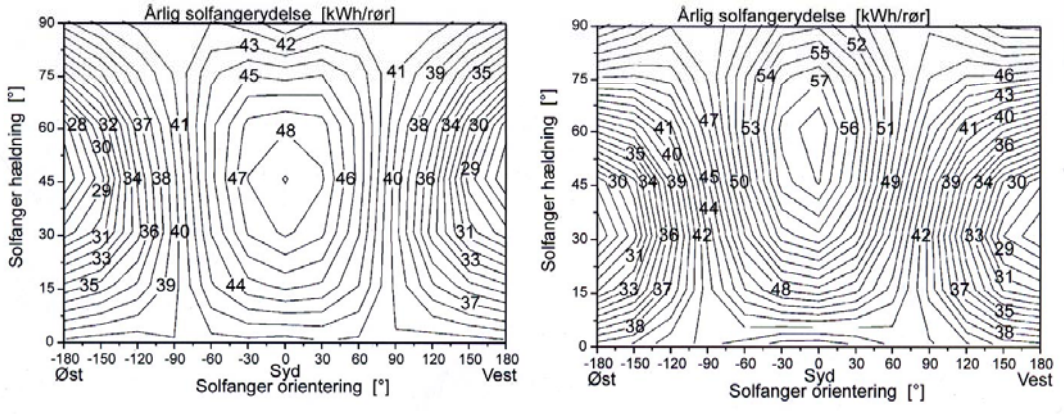

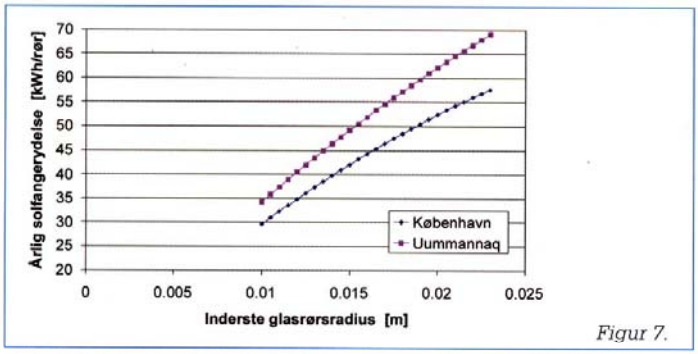

Figur 7.

Følgende parametre er analyseret:

- Solfangerorientering og solfangerhældning (solfangergeometri uændret).
- Radius af inderste glasrør (radius af yderste glasrør uændret).
- Afstand mellem glasrørene (sol fangerorientering og solfangerhældning uændrede).

Hældning

Figur 6 viser solfangerydelsen pr. glasrør som funktion af solfangerhældning og solfangerorientering for hhv. København og Uummannaq.
Figuren viser, at ydelsen falder, når solfangeren orienteres væk fra syd.
Det kan også ses, at den optimale solfangerhældning er ca. 45° for København og ca. 60° for Uummannaq.
Endelig ses det, at ydelserne er noget højere i Uummannaq end i København.
Det skyldes især sneens høje refleksionskoefficient.

Radius

Figur 7 viser solfangerydelsen pr. glasrør ved en solfangermiddeltemperatur på 50°C som funktion af inderste glasrørsradius.
Den ydre glasrørsradius er 0.0235 m.
Figuren viser, at solfangerydelsen stiger med stigende radius.
Stigningen er ikke linær, fordi også varmetabet fra glasrørene stiger med stigende indre glasrørsradius.

Afstand

Endelig viser *figur 8* solfangerydelsen pr. glasrør ved forskellige solfangermiddeltemperaturer, som funktion af afstanden (fra centrum til centrum) mellem glasrørene.
Solfangerydelsen stiger ved større rørafstande indtil en vis afstand på grund af, at rørene skygger mindre for hinanden, jo større rørafstanden er.
Ved endnu større rørafstande falder solfangerydelsen igen. Det skyldes, at varmetabet fra manifoldrørene, som forbinder glasrørene, bliver endnu større end den ekstra ydelse, der hentes på grund af reducerede skygger på glasrørene.
Den optimale rørafstand afhænger af solfangermiddeltemperaturen.
Ved en solfangermiddeltemperatur på 70°C er den optimale afstand ca. 0.15 m og for en solfangermiddeltemperatur på 30°C er den optimale afstand ca. 0.3 m.

Figur 8.

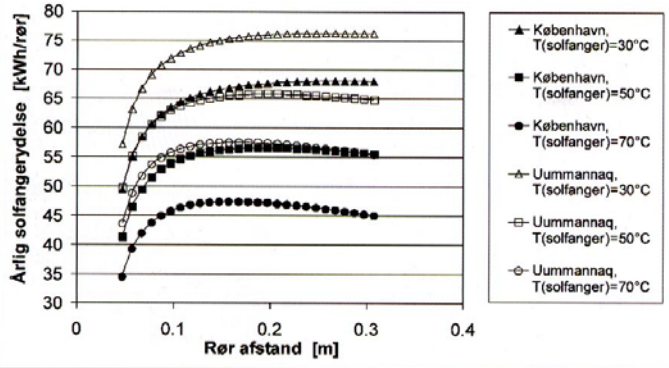

Generelt gælder, at jo højere solfangermiddeltemperaturen er, des mere afgørende bliver varmetabet fra manifoldrørene.

Rentabilitet kan forbedres

Som nævnt er forskningsprojektet ca. halvvejs i forløbet.
Det fortsatte arbejde vil inkludere eksperimentelt arbejde, hvor det bl.a. skal undersøges, hvilket solfangerkoncept (All-glass eller Heat-Pipe), der er mest attraktivt til arktiske forhold.
Det skal i øvrigt nævnes, at vakuumrørsolfangere ikke kun er interessante for arktiske forhold. Det er interessant for alle klimaforhold og for de fleste typer af solvarmeanlæg. Det er bl.a. fordi, der med optimalt designede vakuumrørsolfangere kan være mulighed for at forbedre solvarmeanlægs rentabilitet mærkbart.
Yderligere information om arbejdet udført i forskningsprojektets første år kan findes i [7].

Referencer:

[1] Shah, L.J. & Furbo, S. (2004). *Modelling Shadows on Evacuated Tubular Collectors with Cylindrical Absorbers.* Journal of Solar Energy Engineering, Transactions of the ASME, In press.
[2] Shah, L.J. & Furbo, S. (2004). *Vertical Evacuated Tubular Collectors utilizing solar radiation from all directions.* Applied Energy, Vol. 78/4 pp 371-395, 2004.
[3] Shah, L.J. & Furbo, S. (2005). *Theoretical Investigations of differently designed Heat Pipe Evacuated Tubular Collectors.* Proceedings, ISES Solar World Congress, Orlando, USA. In press.
[4] Klein, S.A. et al. (1996). »TRNSYS 14.2, User Manual«, University of Wisconsin Solar Energy Laboratory.
[5] Lund H. (1995). *The Design Reference Year user manual.* Report of IEA-SHC Task 9. Report 274. Thermal Insulation Laboratory. Technical University of Denmark.
[6] Kragh J. et al (2002). *Grønlandske vejrdata. Nuuk. Uummannaq.* Department of Civil Engineering, Technical University of Denmark. November 2002.
[7] Shah, L.J. (2004). *Bæredygtigt arktisk byggeri i det 21. århundrede. Vakuumrørsolfangere – Statusrapport 1 til Villum Kann Rasmussen Fonden.* BYG.DTU. Sagsrapport SR-04-04.
http://www.byg.dtu.dk/publications/sagsrapporter/byg-sr0404.pdf

Bilag 4: Abstract accepteret til NorthSun 2005 Konferencen: Utilization of Solar Radiation at High Latitudes with Evacuated Tubular Collectors.

UTILIZATION OF SOLAR RADIATION AT HIGH LATITUDES WITH EVACUATED TUBULAR COLLECTORS

Louise Jivan Shah & Simon Furbo
Department of Civil Engineering, Technical University of Denmark
Building 118
DK-2800 Kgs. Lyngby
Denmark
E-mail: ljs@byg.dtu.dk

In this work, theoretical investigations of how evacuated tubular collectors (ETC) with tubular absorbers utilize the solar radiation at high latitudes will be presented. Fig. 1 shows an example of how the tube in such a collector can be designed.

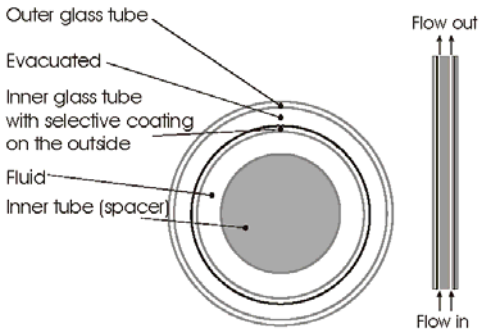

Figure 1: Design of an evacuated tube with a tubular absorber.

The work is based on a new TRNSYS [1] collector model [2, 3] for evacuated tubular collectors with tubular absorbers. The model is based on traditional flat plate collector theory, where the performance equations have been integrated over the whole absorber circumference. On each tube the model determines the size and position of the shadows caused by the neighbour tube as a function of the solar azimuth and zenith.

The input to the model is the exact collector geometry (and not a standard efficiency expression) and it is therefore possible to determine the actual collector geometry's influence on the yearly thermal performance.

The yearly thermal performance of ETC placed in a collector field on the ground will be investigated for three different Nordic climates: Uummannaq (GL), Sisimiut (GL) and Copenhagen (DK). Especially, for the most Nordic locations, Uummannaq and Sisimiut, during summertime solar radiation will be present almost 24 hours a day. This means that the ETC with tubular absorbers might have an extra advantage compared to traditional collectors as they can utilize solar radiation from all directions. For different collector operation conditions and different collector geometries, the investigation will elucidate the daily and yearly distribution of the thermal performance.

References:

[1] Klein, S.A. et al. (1996). *TRNSYS 14.2, User Manual*. University of Wisconsin Solar Energy Laboratory.

[2] Shah, L.J. & Furbo, S. (2004). *Vertical evacuated tubular collectors utilizing solar radiation from all directions*. Applied Energy, Vol. 78/4 pp 371-395.

[3] Shah, L.J. & Furbo, S. (2005). *Modelling Shadows on Evacuated Tubular Collectors with Cylindrical Absorbers*. Journal of Solar Energy Engineering, Transactions of the ASME, In press.

Bilag 5: Overheads til foredraget "*Evacuated Tubular Collectors*".

Energy-Efficient Building, Symposium in Sisimiut, Greenland, April 12-14 2005.

BYG·DTU Department of Civil Engineering

Evacuated Tubular Collectors

Louise Jivan Shah

Background

- 3-year research project
- Part of the research program "Sustainable Arctic Building Technology for the 21st century"
- Funded by the *VILLUM KANN RASMUSSEN FOUNDATION*
- 2/3 through the project

Solar energy at northern latitudes

- Large season variations
- Solar radiation from all directions

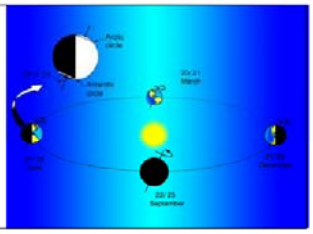

- High ground reflections due to snow
- Low ambient temperatures

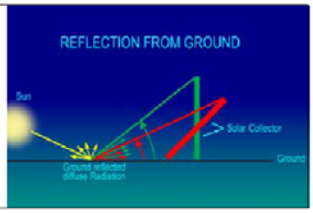

Available solar radiation at northern latitudes

Solar Radiation on horizontal [kWh/m²/year]

- 0-800
- 800-1000
- 1000-1200
- 1200-1400
- 1400-1600

Map Source: UNEP/GRID-Arendal, http://maps.grida.no/arctic/

Solar collectors for northern latitudes

- When solar collectors are developed for northern latitudes, it is an advantage if the collectors:
  - ☺ Can utilize solar radiation from all directions
  - ☺ Have a low heat loss (due to low ambient temperatures)
  - ☺ Utilize ground reflected radiation well (due to large ground reflection coefficient)

Evacuated tubular collectors

- ☺ Low heat loss coefficient
  - Vacuum insulation
- ☺ High efficiency
  - Due to low heat loss
- ☺ Utilize solar radiation from all directions
  - Absorber design

Different principles of evacuated tubular collectors

- Heat pipe evacuated tubular collectors
- All-glass evacuated tubular collectors
- Cheap, mass-produced in China

Two research examples

- Heat pipe evacuated tubular collectors
  - Two different designs in a solar heating plant

- All-glass evacuated tubular collectors
  - Flow and temperature patterns inside the tubes

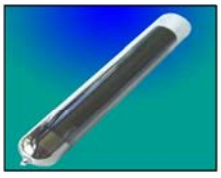

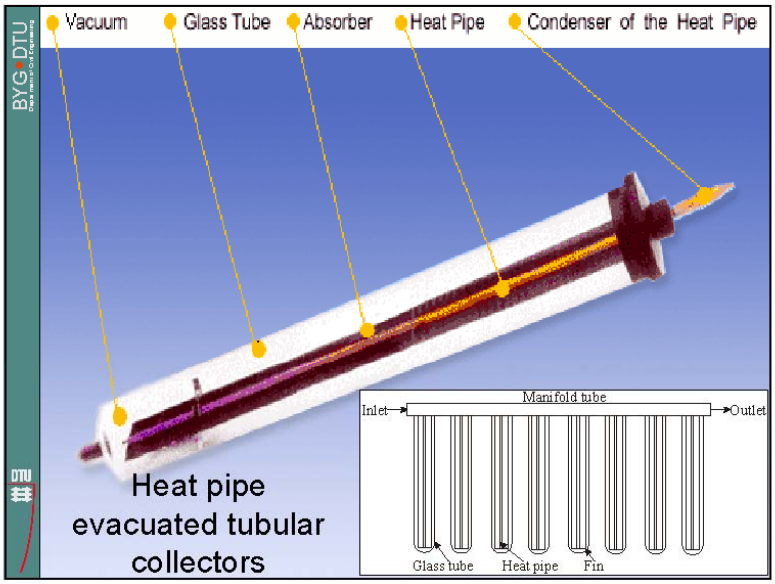
Vacuum
Glass Tube
Absorber
Heat Pipe
Condenser of the Heat Pipe
Heat pipe evacuated tubular collectors
Manifold tube
Inlet
Outlet
Glass tube
Heat pipe
Fin

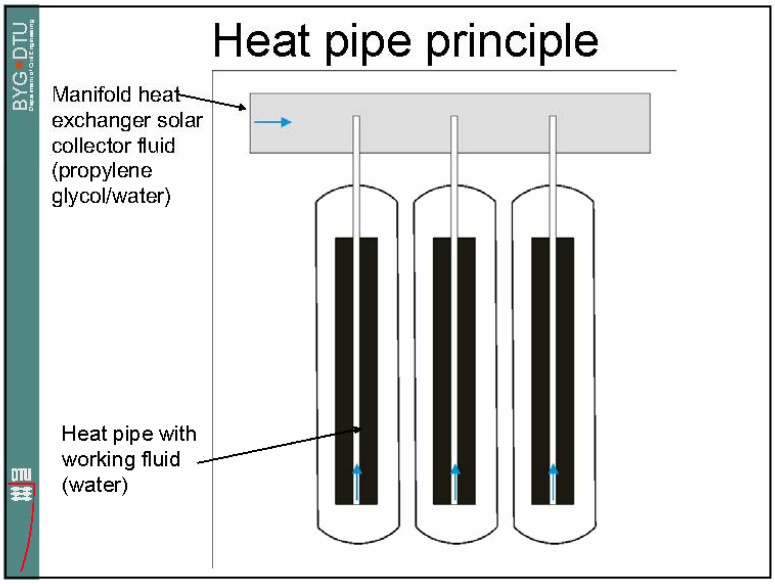
Heat pipe principle
Manifold heat exchanger solar collector fluid (propylene glycol/water)
Heat pipe with working fluid (water)

Heat pipe evacuated tubular collectors with flat or curved fins

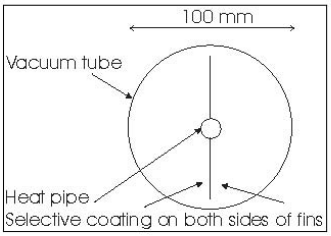

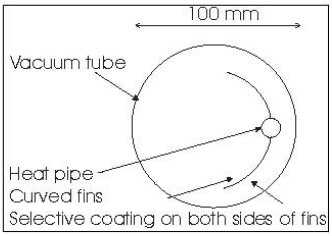

- Research work:
  - New collector theory is developed
  - Calculation yearly thermal performance is now possible
  - Detailed optimization of collector design is now possible

Detailed modeling of shadows temperature distribution

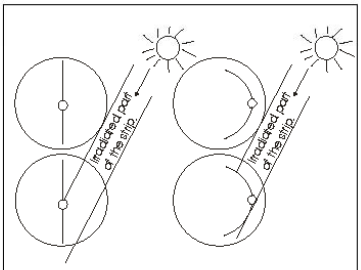

Depending on the position of the sun and the distance between the tubes, the tubes cast shadow on each other

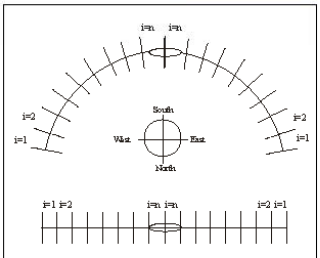

Therefore, the solar irradiance varies along the fin and the fin temperature must be calculated in detail

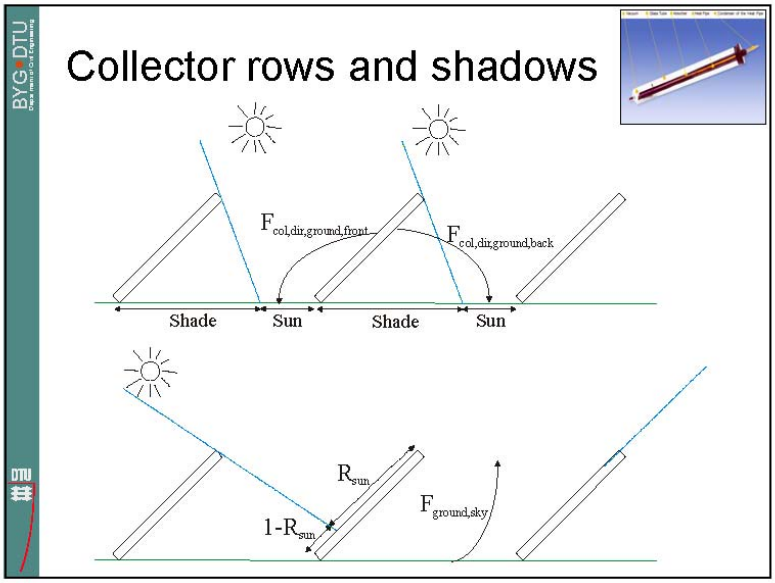
Collector rows and shadows
$F_{col,dir,ground,front}$
$F_{col,dir,ground,back}$
Shade
Sun
Shade
Sun
R_{sun}
$1-R_{sun}$
$F_{ground,sky}$

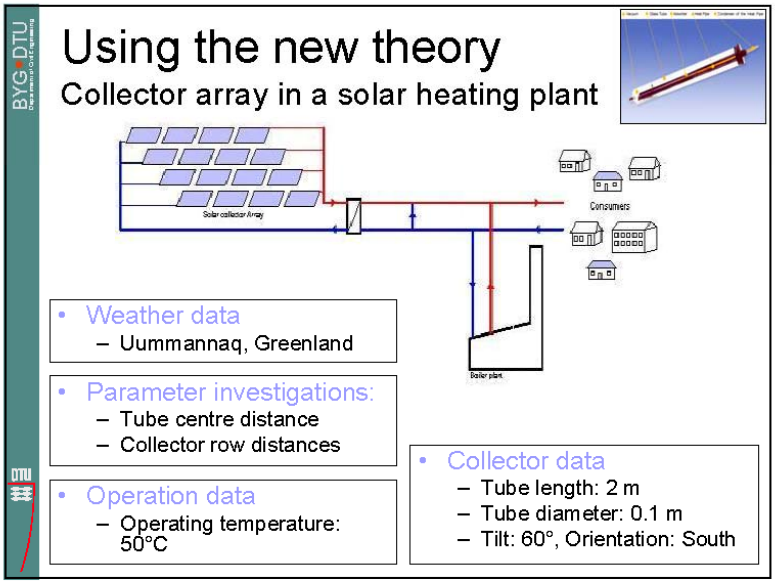
Using the new theory
Collector array in a solar heating plant
Solar collector Array
Consumers
Boiler plant
• Weather data
– Uummannaq, Greenland
• Parameter investigations:
– Tube centre distance
– Collector row distances
• Operation data
– Operating temperature: 50°C
• Collector data
– Tube length: 2 m
– Tube diameter: 0.1 m
– Tilt: 60°, Orientation: South

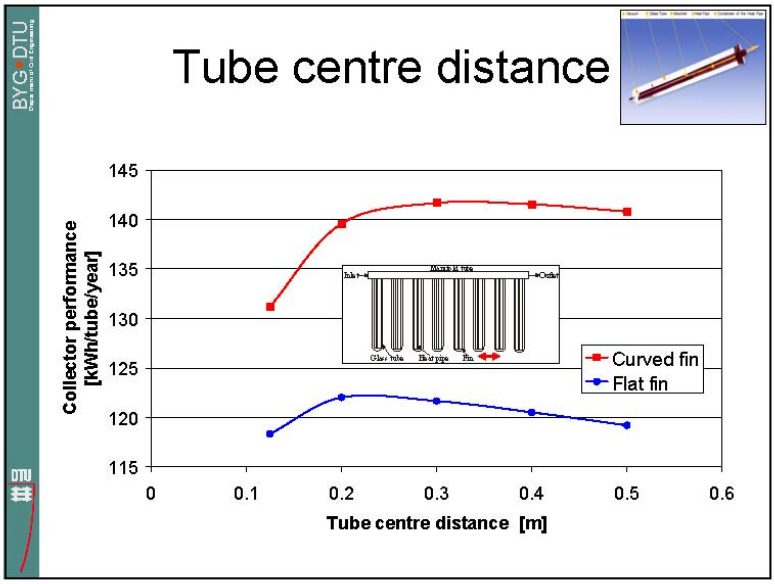
Tube centre distance
Collector performance [kWh/tube/year]
145
140
135
130
125
120
115
0
0.1
0.2
0.3
0.4
0.5
0.6
Tube centre distance [m]
Curved fin
Flat fin

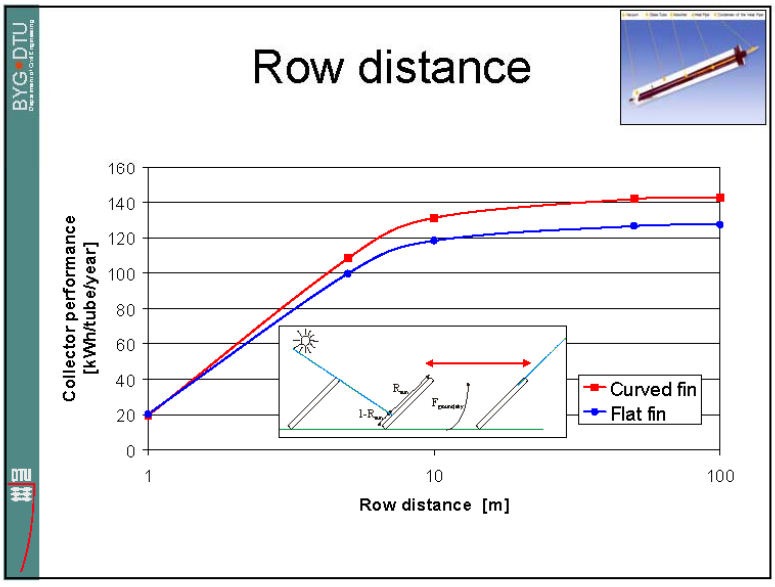
Row distance
Collector performance [kWh/tube/year]
160
140
120
100
80
60
40
20
0
1
10
100
Row distance [m]
Curved fin
Flat fin

Energy production from a solar collector field

- Collector row distance: 5 m
- Tube centre distance: 0.125 m
- 8000 tubes on a ground array with the size of a football court
- Yearly energy production: 1100 MWh/year
- District heating production in Sisimiut: 25000 MWh/year

Summary of research example

- New theory for heat pipe evacuated tubular collectors developed
- The theory includes in detail heat transfer processes of the absorber fins
- Detailed optimization of collector design now possible

All-glass evacuated tubular collectors

Investigation of flow and temperature patterns inside the tubes

- All-glass collector
- Heat transfer
- Flow structures

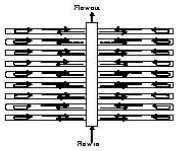

All-glass working principle

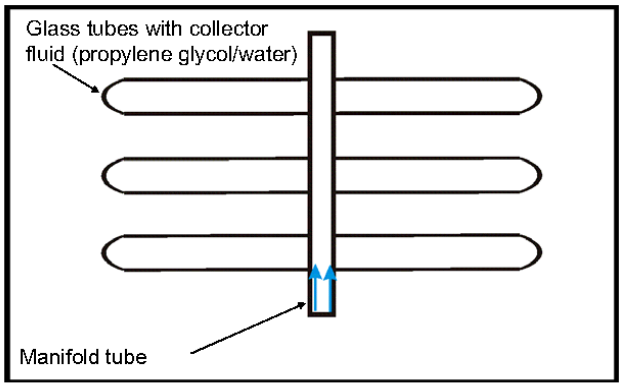

Computational Fluid Dynamics (CFD)

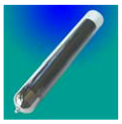

- With CFD temperatures and flow patterns are determined
- A grid is made of the geometry and governing equations of fluid flow are solved numerically

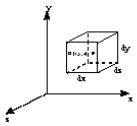

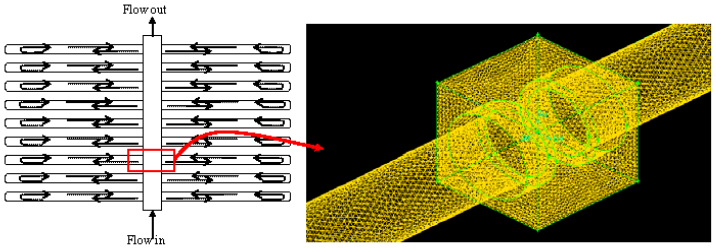

CFD investigations

Calculations:

- 5 different inlet flow rates:
  - 0.05 kg/min – 10 kg/min.
- Inlet temperature: 60 °C
- Typical solar radiation

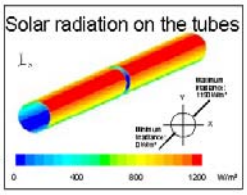

Results:

- Flow structures
- Influence on collector efficiency

Flow inside the All-glass tube

We see two horizontal All-glass tubes connected to the manifold pipe in the centre

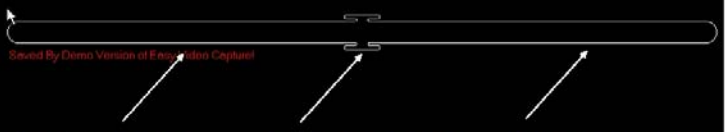

All-glass tube Manifold pipe All-glass tube

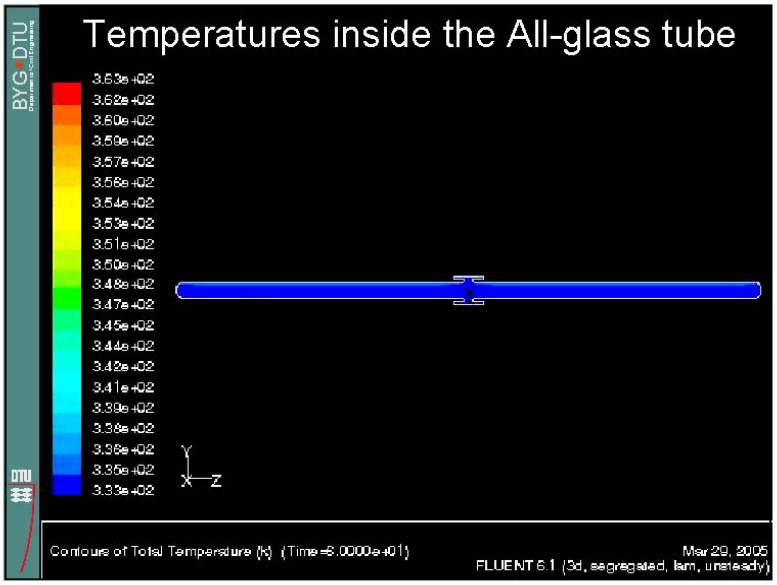
Temperatures inside the All-glass tube
3.63e+02
3.62e+02
3.60e+02
3.59e+02
3.57e+02
3.56e+02
3.54e+02
3.53e+02
3.51e+02
3.50e+02
3.48e+02
3.47e+02
3.45e+02
3.44e+02
3.42e+02
3.41e+02
3.39e+02
3.38e+02
3.36e+02
3.35e+02
3.33e+02
Y
X Z
Contours of Total Temperature (k) (Time=6.0000e+01)
Mar 29, 2005
FLUENT 6.1 (3d, segregated, lam, unsteady)

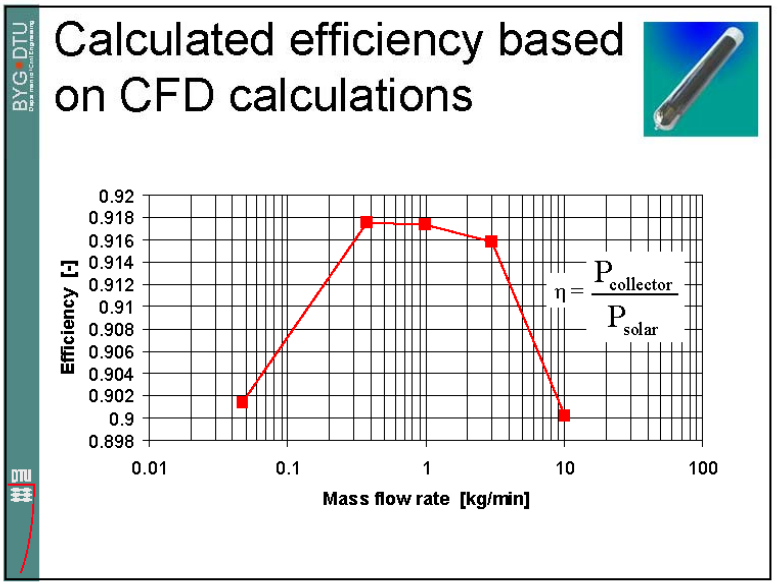
Calculated efficiency based on CFD calculations
Efficiency [-]
0.92
0.918
0.916
0.914
0.912
0.91
0.908
0.906
0.904
0.902
0.9
0.898
0.01
0.1
1
10
100
Mass flow rate [kg/min]
$\eta = \frac{P_{collector}}{P_{solar}}$

Results for different inlet flow rates

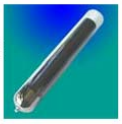

Observation:

- The manifold inlet flow rate has only small (<2%) influence on collector efficiency

Explanation:

- Small variations in the flow patterns in the glass tubes
- Self adjusting flow in glass tubes

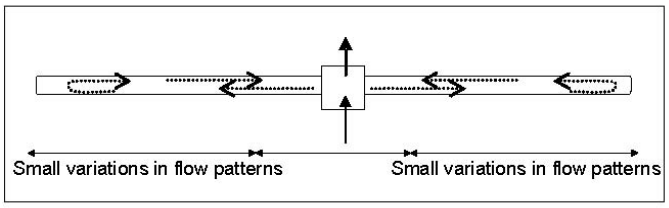

Summary

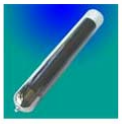

- Example of how Computational Fluid Dynamics gives detailed useful results
- Optimal manifold inlet flow rate is around 0.4-1 kg/min.
- Flow structures in the glass tubes were relatively uninfluenced by the manifold inlet flow rate
- This indicates that the collector design is well working for most operating conditions.

Further work

- Measurements
  - New test facility
  - Test of 5 differently designed evacuated tubular collectors
  - Direct performance comparison
  - Final validation of theoretical models
- Optimization work
- Design
  - Based on the findings and on economy considerations, optimum designed evacuated tubular collectors for Arctic latitudes will be recommended

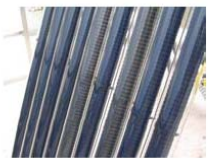

Outlook

- Today, solar heating is one of the largest renewable energy technologies

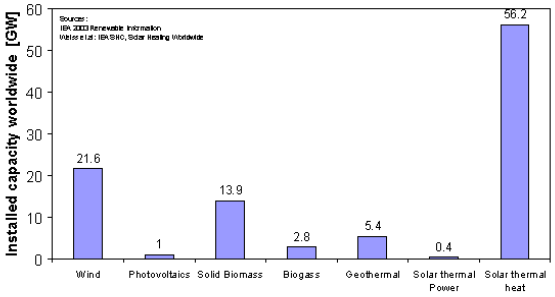

- Maybe, well designed cheap evacuated tubular collectors, will create a shining future for solar heating in Arctic regions

BYG·DTU
Thank you for your attention!

Bilag 6: Overheads/Poster til foredraget ” *New Trnsys Model of Evacuated Tubular Collectors with Cylindrical Absorbers*”.

EuroSun 2004 Congress, Freiburg, Germany, June 20-23, 2004.

BYG·DTU
Department of Civil Engineering

NEW TRNSYS MODEL OF EVACUATED TUBULAR COLLECTOR WITH CYLINDRICAL ABSORBER

Louise Jivan Shah & Simon Furbo
Department of Civil Engineering
Technical University of Denmark
Building 118, DK-2800 Kgs. Lyngby
DENMARK
E-mail: ljs@byg.dtu.dk

Introduction

- A new TRNSYS collector model for evacuated tubular collectors with tubular absorbers is developed
- On each tube the model determines the size and position of the shadows caused by the neighbour tube
- The model takes into account solar radiation from all directions (also from the "back" of the collector)
- The model is validated with measurements
- The model makes it possible to make a theoretical design optimization

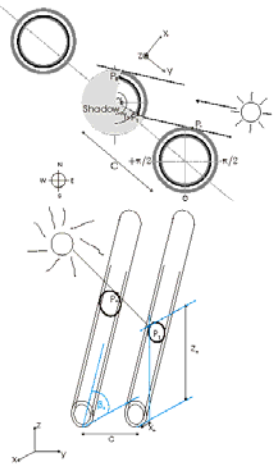

I look forward to meet you at the poster where you can see some calculation examples

NEW TRNSYS MODEL OF EVACUATED TUBULAR COLLECTOR WITH CYLINDRICAL ABSORBER

L.J. Shah & S. Furbo, BYG.DTU, Technical University of Denmark, Email: ljs@byg.dtu.dk

Summary

A new TRNSYS collector model for evacuated tubular collectors with tubular absorbers is developed.

The model is based on traditional flat plate collector theory, where the performance equations have been integrated over the whole absorber circumference.

On each tube the model determines the size and position of the shadows caused by the neighbour tube as a function of the solar azimuth and zenith.

The model takes into account solar radiation from all directions (also from the "back" of the collector)

Calculations with the new model of a tubular collector are compared with measured results and a good degree of similarity between the measured and calculated results is found.

The collector model is used in a model of a solar heating plant and a sensitivity analysis of the tube centre distance, collector tilt and orientation with respect the thermal performance per tube is investigated for the two locations Copenhagen (Denmark) and Uummannaq (Greenland).

On each tube the model determines the size and position of the shadows caused by the neighbour tube as a function of the solar azimuth and zenith

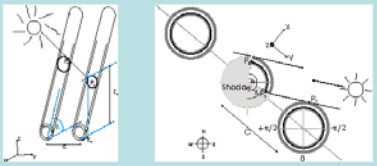

Prototype panel and model validation

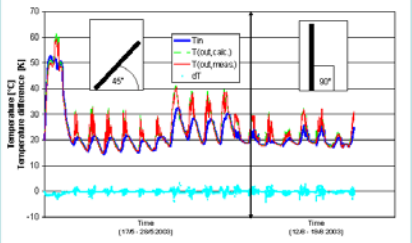

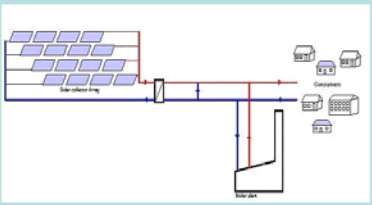

Simulation of solar heating plants.

A model of a solar heating plant is built in TRNSYS. The collector array consists of 100 rows – 50 m long.

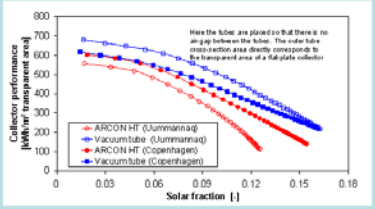

The thermal performance per tube as a function of the tube centre distance, collector tilt and orientation (Copenhagen).

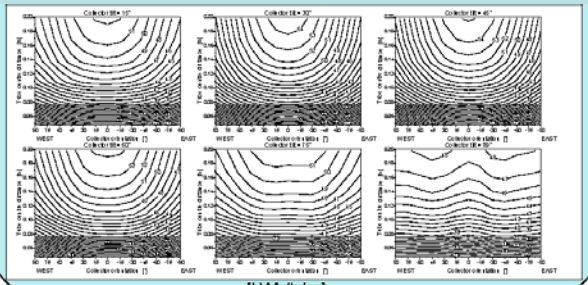

[kWh/tube]

The thermal performance per tube as a function of the tube centre distance, collector tilt and orientation (Uummannaq).

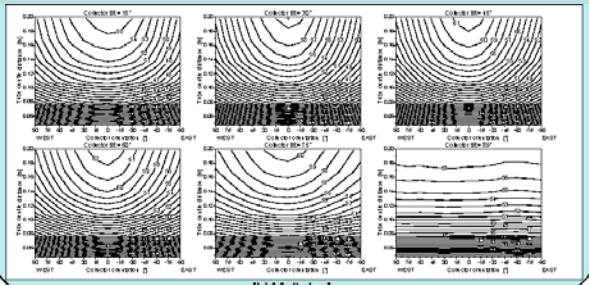

[kWh/tube]